



# **Potential of Commercial Air Quality Sensors to Detect Bleed Air Contamination Events**

Final Report

R.A. Overfelt, J.R. Andress, R.L. Haney, R.L. Neer, M.I. Roberts, A.L. Buck,  
M.S. Crumpler and B.C. Brooks

National Air Transportation Center of Excellence for  
Research in the Intermodal Transport Environment (RITE)  
Airliner Cabin Environment Research Program  
Auburn University  
Auburn, AL 36849

August 17, 2015

Report No. RITE-ACER-CoE-2015-1

## NOTICE

---

This document is disseminated under the sponsorship of the U.S. Department of Transportation in the interest of information exchange. The United States Government assumes no liability for the contents thereof.

---

This work was funded by the U.S Federal Aviation Administration Office of Aerospace Medicine under Cooperative Agreement 10-C-RITE.

---

This publication is available in full-text from the publications Web site of the National Air Transportation Center of Excellence for Research in the Intermodal Transport Environment (RITE) at:  
*[www.acer-coe.org](http://www.acer-coe.org)*

### Technical Report Documentation Page

1. Report No. RITE-ACER-CoE-2015-1	2. Government Accession No.	3. Recipient's Catalog No.	
4. Title and Subtitle Potential of Commercial Air Quality Sensors to Detect Bleed Air Contamination Events		5. Report Date August 17, 2015	
		6. Performing Organization Code	
7. Author(s) R.A. Overfelt, J.R. Andress, R.L. Haney, R.L. Neer, M.I. Roberts, A.L. Buck, M.S. Crumpler and B.C. Brooks		8. Performing Organization Report No.	
9. Performing Organization Name and Address National Air Transportation Center of Excellence for Research in the Intermodal Transport Environment Auburn University Auburn, AL 36849		10. Work Unit No. (TRAIS)	
		11. Contract or Grant No. FAA Cooperative Agreement 10-C-RITE	
12. Sponsoring Agency name and Address FAA Office of Aerospace Medicine 800 Independence Ave., S.W. Washington, DC 20591		13. Type of Report and Period Covered	
		14. Sponsoring Agency Code	
15. Supplemental Notes Work was accomplished under Public law 108-76.			
16. Abstract Most environmental control systems on commercial airliners receive fresh outside air from the bleed air systems of the compressors of the jet engines or from the auxiliary power units. Although outside air is clean and sterile during cruise conditions at flight altitudes, spurious air contamination events have been reported. Bleed air supplies can be contaminated during ground operations by de-icing fluids entering the bleed air supply. Engine oil from worn mechanical seals and hydraulic fluids have also been reported to contaminate the bleed air supply. This document provides the findings of an investigation on the potential of commercial air quality sensors to measure levels of carbon monoxide and carbon dioxide in aircraft. In addition, a high sensitivity electrochemical carbon monoxide sensor from Alphasense (CO-B4) detected the presence of carbon monoxide in the bleed air supply of a Pratt & Whitney F117/PW2000 engine from controlled injections of Mobil Jet Oil II (10 g/min – 20 g/min) into the engines AP1 borescope port. This technology has potential for development into engine oil contamination detector for aircraft bleed air supplies.			
17. Key Words Sensors, aircraft, bleed air, contamination, detector		18. Distribution Statement	
19. Security Classif. (of this report) Unclassified	20. Security Classif. (of this page) Unclassified	21. No. of Pages 45	22. Price

## CONTENTS

Nomenclature .....	ii
List of Tables .....	iv
List of Figures .....	iv
1.0 Background and Introduction .....	1
2.0 Review of Previous Research .....	4
2.1 Overview of Aircraft Bleed Air Supply Systems .....	4
2.2 Thermal Degradation of Aircraft Working Fluids .....	5
2.3 Summary of Gaseous Contaminant Targets for Detection .....	7
2.4 Review of Commercial Gas Sensing Technologies .....	8
3.0 Methods and Materials .....	13
3.1 Evolved Gas Analysis by TGA/FTIR/MS .....	13
3.2 Variable Pressure Commercial Sensor Test System .....	14
3.3 Steady State Testing of Commercial CO and CO <sub>2</sub> Sensors .....	15
3.4 Transient Testing of Commercial CO and CO <sub>2</sub> Sensors .....	17
4.0 Results and Discussion .....	19
4.1 Characterization of Fumes from Oil Degradation Experiments .....	19
4.2 Commercial CO and CO <sub>2</sub> Sensor Response Characterization .....	25
4.2.1 Steady State Responses to Calibration Gases .....	25
4.2.1.1 NDIR CO <sub>2</sub> Sensors .....	25
4.2.1.2 Electrochemical CO Sensors .....	28
4.2.2 Transient Responses to Calibration Gases .....	30
4.2.2.1 NDIR CO <sub>2</sub> Sensors .....	30
4.2.2.2 Electrochemical CO Sensors .....	34
4.3 Commercial Sensors' Responses to Fumes from Mobil Jet Oil II .....	35
4.4 Detection of Bleed Air Contamination from Mobil Jet Oil II Injection into the AP1 Port of a Pratt & Whitney F117/PW2000 Turbofan Engine .....	37
5.0 Conclusions .....	42
6.0 Acknowledgments .....	43
7.0 References .....	43

## Nomenclature

AIDS	= Accident/Incident Data System
amu	= atomic mass unit
APU	= auxiliary power unit
ASHRAE	= American Society of Heating, Refrigeration and Air-Conditioning Engineers
ASIAS	= Aviation Safety Information Analysis and Sharing
ASRS	= Aviation Safety Reporting System
BP	= British Petroleum
C	= Celsius
cfm	= cubic feet per minute
CFR	= Code of Federal Regulations
CO	= carbon monoxide
CO <sub>2</sub>	= carbon dioxide
DOT	= Department of Transportation
DTA	= differential thermal analysis
EPA	= Environmental Protection Agency
eV	= electron volts
FAA	= Federal Aviation Administration
FAR	= Federal Aviation Regulation
FTIR	= Fourier Transform Infra-red
GC	= gas chromatography
HVAC	= heating, ventilating and air conditioning
IR	= infrared
L	= liter
M	= molar
MEMS	= microelectromechanical system
mg	= milligram (10 <sup>-3</sup> g)
min	= minute
mL	= milliliter (10 <sup>-3</sup> L)
MOS	= metal oxide semiconductor
MPa	= mega-Pascal (10 <sup>6</sup> Pa)
MS	= mass spectrometry
NAAQS	= National Ambient Air Quality Standards
NASA	= National Aeronautics and Space Administration
NDIR	= non-dispersive infrared
O <sub>2</sub>	= oxygen
O <sub>3</sub>	= ozone
OSHA	= Occupational Safety and Health Agency
PEL	= permissible exposure limit
PID	= photoionization detector
PM <sub>2.5</sub>	= particulate matter less than 2.5 X 10 <sup>-6</sup> m (2.5 microns) in diameter
PM <sub>10</sub>	= particulate matter less than 10 X 10 <sup>-6</sup> m (10 microns) in diameter
PMMA	= polymethyl methacrylate
ppbv	= parts per billion by volume
ppm	= parts per million

ppmv	= parts per million by volume
rms	= root-mean-squared
SDRs	= Service Difficulty Reports
SDRS	= Service Difficulty Reporting System
SnO <sub>2</sub>	= tin oxide
SQL	= Structured Query Language
T90	= time for a sensor response to achieve 90% of the final steady state value
TCP	= tri-cresyl phosphate
TGA	= thermogravimetric analysis
UV	= ultraviolet
VOC	= volatile organic compound
$\mu\text{g}/\text{m}^3$	= $10^{-6}$ g per cubic meter
$\mu\text{L}$	= $10^{-6}$ L

## List of Tables

Table I	Applicable Air Quality Standards: Ambient Air, Workplaces and Aircraft .....	2
Table II	Summary of Potential Bleed Air Contaminants .....	8
Table III	Possible Bleed Air Contaminants and Potential Sensor Technologies .....	12
Table IV	Jet Engine Oils: Peak Degradation Temperatures .....	21
Table V	Pressure Sensitivity of Commercial NDIR CO <sub>2</sub> Sensors .....	27
Table VI	Summary of the Accuracy of Each Discrete CO <sub>2</sub> Sensor .....	31
Table VII	Summary of RMS Noise evaluation of Each Discrete CO <sub>2</sub> Sensor .....	31
Table VIII	Summary of RMS Noise of Each Discrete CO <sub>2</sub> Sensor (1 sec running average) ...	32
Table IX	Limits of Detection for Each Discrete CO <sub>2</sub> Sensor .....	33
Table X	T <sub>90</sub> Response Times for Each Discrete CO <sub>2</sub> Sensor .....	34
Table XI	Transient Performance for Discrete CO Sensors .....	34
Table XII	Commercial Sensors Evaluated in the VIPR Bleed Air Contamination Tests .....	39

## List of Figures

Figure 1.	Typical Airliner Bleed Air Supply System adapted from [12]	5
Figure 2.	Modern aircraft turbofan jet engine: location of the compressor bleed air lines and the bleed air pre-cooler [13]	5
Figure 3.	TGA and DTA plots of pentaerythritol derivative in air [17]. The low temperature exothermic peak at about 350°C corresponds to low temperature oxidation producing smoke, low molecular weight hydrocarbons, CO and CO <sub>2</sub> . The higher temperature exothermic peak corresponds to oxidation of the remaining oil and charred oil to smoke, CO and CO <sub>2</sub> .	7
Figure 4.	Schematic representation of commercial gas sensor detection technologies. (a) catalytic bead sensors typically used to detect inflammable gases; (b) conductometric sensors based upon metal-oxide semiconductor materials; (c) 3-electrode configuration of electrochemical sensors; (d) Schematic representation of photoionization detectors for detecting volatile organic compounds like benzene, ethanol, acetone, amines and ammonia; and (e) two channel non-dispersive infra-red (NDIR) sensor often used for measuring CO <sub>2</sub> in HVAC systems. Schematics (a) and (d) adapted from [21]	10
Figure 5.	Evolved gas analysis experimental arrangement used by NETZSCH Instruments Applications Laboratory.	13
Figure 6.	Experimental arrangement for testing commercial CO and CO <sub>2</sub> sensors	14
Figure 7.	CO sensors and evaluation boards investigated in this work: Alphasense CO-B4, Figaro TGS5042 and e2v EC4-500-CO	16
Figure 8.	Schematic and picture of the experimental arrangement for transient testing of commercial CO sensors	17
Figure 9.	Schematic of the desired instantaneous gas concentration profile (dashed line) compared with an expected sensor response (solid line)	17
Figure 10.	CO <sub>2</sub> sensors and evaluation boards investigated: Madur madIR-DO1 CO <sub>2</sub> , E2V IR11EJ, Figaro K30	18
Figure 11.	Overall arrangement of the experimental apparatus for transient testing of commercial CO <sub>2</sub> sensors	18
Figure 12.	Mass changes of BP274 oil sample as a function of exposure temperature. Sample size = 5.46 mg and 10°C/min heating rate in air.	19

Figure 13. Time dependent mass loss and sample temperature data shown with mass spectrometry ion-currents for the following evolved gaseous species: (a) 2 amu – H<sub>2</sub>, 12 amu - C, 17 and 18 amu – H<sub>2</sub>O, 44 amu – CO<sub>2</sub>; (b) 32 amu – CH<sub>3</sub>OH, 29 amu – C<sub>2</sub>H<sub>5</sub>, 31 amu – CH<sub>2</sub>OH, 34 amu – H<sub>2</sub>S, 30 amu – C<sub>2</sub>H<sub>6</sub>, 43 amu – C<sub>3</sub>H<sub>7</sub>, and 39 amu – C<sub>3</sub>H<sub>3</sub>. ..... 20

Figure 14. 3D plot of gas evolution FTIR absorbance data versus time for BP274 sample. ... 21

Figure 15. (a) FTIR scans of BP Turbo Oil 274(301°C), BP Turbo Oil 2380(305°C), Aeroshell Turbine Oil 560 (326°C) and Mobil Jet Oil II (307°C) at the indicated temperatures of greatest mass loss. The order of the data in each peak from each oil sample is indicated by the listing adjacent to the peak. (b) Pure theoretical spectra from various possible components of the evolving gas mixture. The infrared bond excitation regions are also indicated. .... 23

Figure 16. Experimental and calculated FTIR spectra and predicted evolved gas compositions at the times indicated during thermal degradation of BP Turbo Oil 2380. See the text for a discussion of the calculation procedures [32] ..... 24

Figure 17. Laboratory FTIR and commercial CO<sub>2</sub> NDIR sensor responses to introduction of 1340 ppm CO<sub>2</sub> in nitrogen at 0.67 atm pressure in the test chamber (10,780 ft equivalent altitude). Indicated time is from the beginning of introduction of the test gas. Test gas flow stopped at 200 min ..... 26

Figure 18. Theoretical pressure sensitivity (triangles) of the CO<sub>2</sub> partial pressure calculated assuming ideal gas behavior compared to sensor indications from a typical NDIR CO<sub>2</sub> sensor (diamonds: Johnson Controls CD-WA0). Note that the commercial sensor exhibits a higher sensitivity to pressure than expected from theoretical considerations ..... 27

Figure 19. Experimental measurements of CO concentration in nitrogen (mg CO per m<sup>3</sup>) for the electrochemical sensors indicated versus known concentrations in pure nitrogen test gases at the following pressures: (a) 101.3 kPa, (b) 87.5 kPa and (c) 75.3 kPa [33] ..... 28

Figure 20. Repeated transient measurements of CO concentration in simulated air (80% nitrogen and 20% oxygen) for the electrochemical sensors indicated versus known concentrations in pure nitrogen test gases. [33] ..... 29

Figure 21. Three repeated transient measurements of CO concentration (known value = 233 mg CO per m<sup>3</sup>) in simulated air (80% nitrogen and 20% oxygen) at 101.3 kPa for the electrochemical sensors indicated. The calculated transient test chamber concentration is shown by the dashed line. [33] ..... 30

Figure 22. Schematic response of a NDIR CO<sub>2</sub> sensor to a flowing gas experiment illustrating the two transient parameters: (i) time to detection and (ii) time to reach 90% of the new steady state concentration (T<sub>90</sub>). The gas concentration is instantaneously changed to a new steady value when the time = zero. ....32

Figure 23. Steady state comparison of the CO-B4 (triangles), Figaro TGS5042 (squares), and e2v EC4-500-CO (circles). The sensor readings were compared with the actual concentration and the ideal 1:1 relationship (solid). ....34

Figure 24. Bell jar: (a) before thermally degrading 1g of Mobil Jet Oil II; (b) smoke-filled bell jar during degradation experiment [34]..... 35

Figure 25. Plot of the change in CO concentration as a function of time as measured by the TGS5042 sensor (circles) and the FTIR (diamonds) and the mass (dashes) as a function of time. [34] ..... 36

Figure 26. Plot of the CO<sub>2</sub> concentration as a function of time as measured by the EE80 (circles) and the FTIR (diamonds) and the mass (dashes) as a function of time. [34] ..... 36

Figure 27. (a) Overall configuration of the C17 engine test systems. (b) Schematic of the layout for the oil injection system and the commercial sensor bleed air test system. .... 38

Figure 28. (a) Picture of the main components of the oil injection system. (b) Picture of the commercial sensor test system . ....39

Figure 29. Amounts of carbon monoxide (CO) detected with the Alphasense CO-B4 high sensitivity sensor (upper curve) and the measured amounts of oil injected into the engine (lower curve) during Day 1 of the VIPR tests. Partial clogging of the miniature oil injector nozzle caused poor control of the amount of oil injection....40

Figure 30. Amounts of carbon monoxide (CO) measured with the Alphasense CO-B4 high sensitivity sensor (upper curve) and the measured amounts of oil injected into the engine (lower curve) during Day 2 of the VIPR tests. ....41

## 1.0 Background and Introduction

The Federal Aviation Regulations (FARs) implement the FAA's various safety and health requirements. Relevant aspects for the design and operation of commercial aircraft are contained in "Title 14 - Aeronautics and Space" of the Code of Federal Regulations (i.e., 14 CFR). Part 25 of 14 CFR provides the aircraft design standards for transport category airplanes while Part 121 of 14 CFR contains the operating requirements for air carriers and commercial operators.

These regulations provide the FAA's air quality standards with respect to aircraft cabin ventilation and pressure as well as maximum amounts of potential air quality contaminants. Airliner cabins are typically supplied outside air at rates of about 8-16 cfm per passenger and total air exchanges average approximately 15-25 cabin air exchanges per hour [1]. Table I compares the federal ambient air quality standards of the EPA with OSHA's corresponding workplace standards and the FAA limits for aircraft. While 14 CFR 25.831 states that aircraft air must be free from harmful or hazardous concentrations of gases or vapors and 14 CFR 121.219 notes that fumes from fuel may not be present in the air, the FAA specifically only limits the following: (i) ozone, (ii) carbon monoxide and (iii) carbon dioxide. Even with specific allowable limits, there are currently no requirements for real-time monitoring of any of these contaminants on aircraft.

Aircraft air supplies can be contaminated during ground operations by exhaust fumes from the engines of nearby aircraft or perhaps by de-icing fluids entering the outside air supply. One example of such an event occurred in December 2008 when de-icer fumes entered the cabin of an Alaskan Airlines plane. Seven crew members were sent to the hospital and 18 passengers were treated on-sight for eye irritation, dizziness, and nausea [2]. Although outside air is clean and sterile during cruise conditions at flight altitudes, spurious air contamination events have also been reported during flight [1, 3-5] due to engine oils and/or hydraulic fluids from worn mechanical seals or overfilled sumps. For example, a suspected hydraulic fluid leak in January 2010 on a U.S. Airways flight is believed responsible for fumes entering the cabin of the airplane. Passengers and crew members complained of headaches and nausea [5]. Engine oil contamination of the air supply is particularly worrisome since some engine oils contain 1-5% tricresyl phosphate, a wear-reduction additive and potential health hazard [6,7]. Given the very high air flow rates and high temperatures in the upstream portion of the bleed air system, the specific nature and extent of potential decomposition reactions of engine oils and hydraulic fluids are largely unknown. In addition, the resulting nature and potential toxicity of any contaminants in the aircraft cabin from such events are highly speculative at the present time.

In 2009 Watson conducted an internal FAA review of records to ascertain the number of bleed air contamination events within the domestic air transportation system [8]. The FAA Aviation Safety Information Analysis and Sharing (ASIAS) system is composed of multiple databases including the Accident/Incident Data System (AIDS) and the Service Difficulty Reporting System (SDRS). The FAA review of the SDRS database covered January 1999 - November 2008 and looked for event records that contained the following identification terms: "odor, smell or fume." The search found 252 air contamination events where failures occurred in "airplane, engine or auxiliary power unit systems that may have caused tri-cresyl phosphate lubricants or

phosphate ester hydraulic fluids or fuel or products of combustion of these fluids to enter the cockpit/cabin ventilation systems.” Of these 252 reported incidents, 33% were due to fuel leaks, 23% were from propulsion engine oil leaks, 18% were from APU oil leaks, 13% were due to air cycle machine oil leaks and 13% were due to hydraulic fluid leaks. During this same period of time, there were 93,647,734 corresponding aircraft departures. Thus the event rate is of the order of 2.7 events per million aircraft departures. Watson noted the “trial-and-error” nature of maintenance diagnostics for such events. In several cases, multiple events were recorded in the SDRS database for the same aircraft before the problem was properly diagnosed and then satisfactorily resolved by maintenance crews.

**Table I**  
**Applicable Air Quality Standards: Ambient Air, Workplaces and Aircraft**

<i>Pollutant</i>	<i>Ambient Standard EPA NAAQS 40 CFR</i>	<i>Workplace Standard OSHA PEL</i>	<i>Aircraft Standard FAA - 14 CFR</i>
Ozone	0.12 ppmv 1-hr 0.08 ppmv 8-hr	0.1 ppmv	0.1 ppmv* 0.25 ppmv**
Carbon Monoxide	35 ppmv 1-hr 9 ppmv 8-hr	50 ppmv	50 ppmv <sup>#</sup>
Carbon Dioxide	NA	5000 ppmv	5000 ppmv <sup>#</sup>
PM <sub>10</sub>	150 µg/m <sup>3</sup> 24-hr	NA	NA
PM <sub>2.5</sub>	65 µg/m <sup>3</sup> 24-hr	NA	NA

\* “0.1 parts per million by volume, sea level equivalent, time weighted average during any 3-hr interval” – 14 CFR 25.832

\*\* “0.25 parts per million by volume, sea level equivalent, at any time above 32,000 ft” – 14 CFR 25.832

# - 14 CFR 25.831

Murawski and Supplee [9] examined the AIDS and SDRS databases over an 18 month period from January 2006 through June 2007. These researchers supplemented the federal databases with additional data from aircraft flight attendant labor union records as well as publically available newspaper reports. Their search looked for records containing the following complaint terms: fume, haze, mist, odor, smell or smoke. In addition, the search also included reports of engine oil maintenance issues that did not explicitly mention an air contamination issue. (It is unclear how the authors decided to include such records into their data set.) Murawski and Supplee concluded that 0.86 events occurred each day during the 18 month study period. With approximately 26,060 U.S. aircraft departures per day in 2006 [10], the event rate for 2006 was estimated to be of the order of 33 events per million aircraft departures. This finding is about an order of magnitude greater than that found by Watson [8].

In 2008, the American Society of Heating, Refrigeration and Air-Conditioning Engineers (ASHRAE) published ASHRAE Standard 161-2007, “Air Quality within Commercial Aircraft” [10]. The standard discusses multiple possible sources of air contamination on aircraft and mandates installation of “one or more” sensors to detect “partly or fully pyrolyzed engine oil or hydraulic fluid” in the bleed air system. However, the standard does not define specifically what should be monitored nor how it should be monitored. Research is needed to establish that specific chemical air contaminants can be identified that are indicative of a bleed air contamination event and that sensor technologies can be developed to reliably detect such events.

## 2.0 Review of Previous Research

### 2.1 Overview of Aircraft Bleed Air Supply Systems

An airliner environmental control system (ECS) is designed to (i) pressurize the cabin, (ii) regulate the temperature of the aircraft within acceptable limits of comfort and safety, (iii) provide fresh air to the occupants, (iv) flush gaseous air contaminants overboard and, to some extent, (v) control humidity in the air supply. Except for the new Boeing 787, most aircraft environmental control systems are designed for constant volumetric flow during flight. In addition, the systems often utilize approximately 30-55% re-circulated air to maximize energy efficiency and receive fresh outside air from the bleed air systems of the compressors of the propulsion engines. Typical aircraft systems are not designed for proportional control and are either simply ON or OFF. Although the re-circulated air is often filtered with high-efficiency particulate filters that capture 99.7% of all particles larger than 0.3  $\mu\text{m}$ , the reliance on re-circulated air in aircraft to meet ventilation requirements has been criticized in the popular press.

Figure 1 shows a schematic of a high-bypass fan jet engine bleed air system which is typical for commercial airliners [12]. Hot compressed air is taken from the engine compressor and cooled in the pre-cooler to temperatures around 175°C before being supplied to the environmental control system and other functions on the aircraft. Modern engines have two bleed air ports at different stages of the compressor in order to minimize excess temperature and pressure in the bleed air and to maximize engine energy efficiency. The actual temperature and pressure of the air exiting the engine compressor can be as high as 350°C and 1.2 MPa or as low as 185°C and 0.21 MPa depending upon the phase of flight and engine operation [1]. If the aircraft is equipped with an ozone converter, the converter is normally located downstream of the pre-cooler but before the air is further cooled to cabin temperatures since most ozone converters work best at elevated temperatures. The pre-cooler is a cross-flow, air-to-air heat exchanger located in the engine pylon just aft of the fan and immediately above the engine compressor as shown in Figure 2 [13]. The pre-cooler uses ducted fan air to cool the hot bleed air from the compressor. The bleed air lines from the engine to the pre-cooler are not long so that the exposure times of potential contaminants to the highest temperatures could be very brief. Chemical reaction kinetics are expected to play an important role in the reactions that occur with the contaminants in the bleed air. Most of the important chemical reactions should occur either within the engine compressor itself or in the hot section of the bleed air path between the compressor and pre-cooler.

The air from the bleed air system shown in Figure 1 is directed to the cabin through air-conditioning packs where the air is further cooled in air cycle machines. The air from the air-conditioning packs is then directed to the mixing manifold where it is mixed with cabin recirculation air for distribution throughout the aircraft.

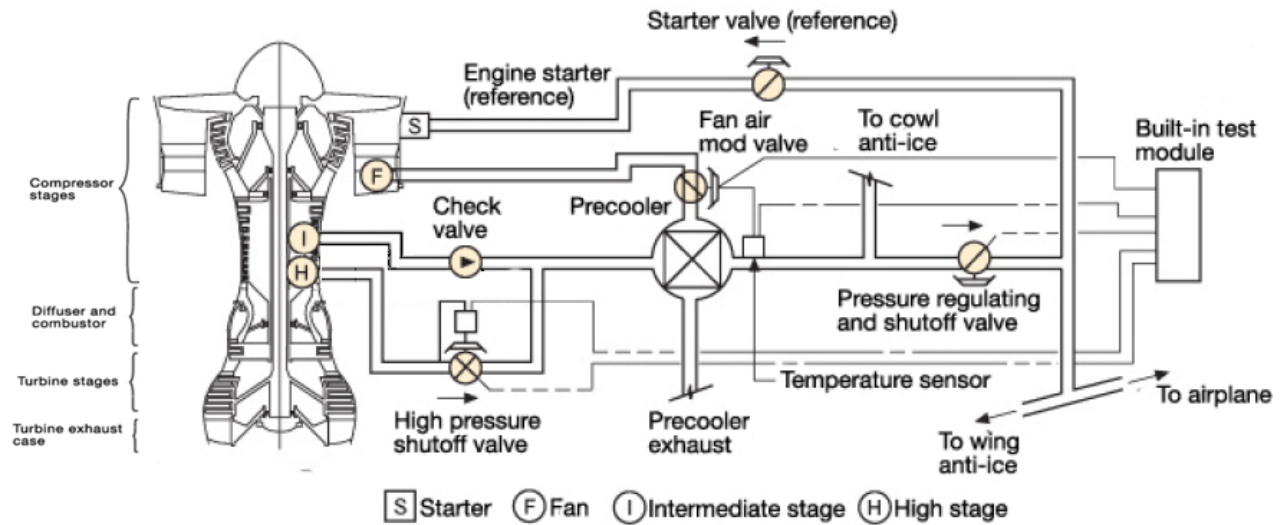


Figure 1. Typical Airliner Bleed Air Supply System adapted from [12].

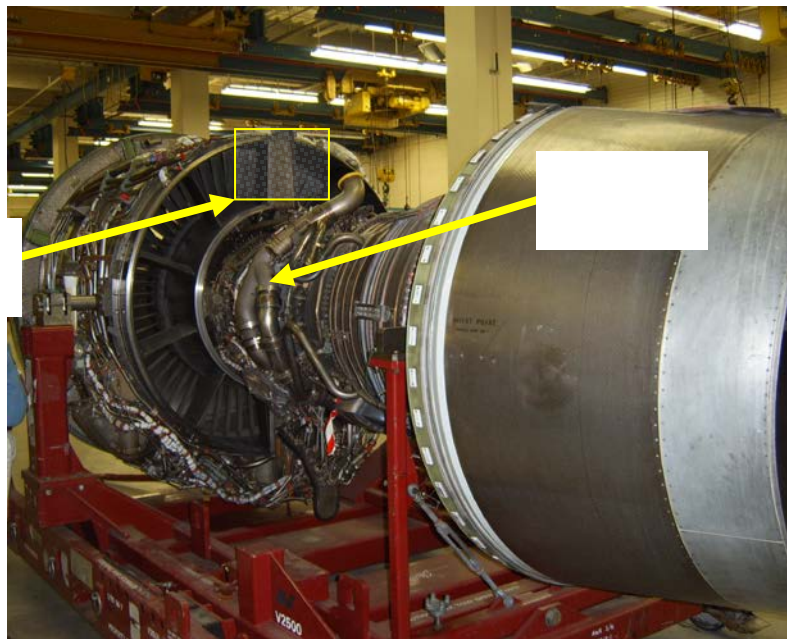


Figure 2. Modern aircraft turbofan jet engine: location of the compressor bleed air lines and the bleed air pre-cooler [13].

## 2.2 Thermal Degradation of Aircraft Working Fluids

Van Netten *et al.* [14-16] evaluated the thermal degradation of a number of hydraulic fluids and jet engine oils during heating on a ceramic hot plate. A thermocouple was used to monitor the temperature of the hot plate. Gases were evolved into a 250 L stainless steel chamber equipped

with a multigas monitor TMX-412 (Industrial Scientific Corporation, Oakdale, PA) to measure NO<sub>2</sub>, oxygen (O<sub>2</sub>), and carbon monoxide (CO). Additionally, a YES-204A monitor (Young Environmental Systems, Richmond, B.C., Canada) was also located in the chamber to measure temperature, relative humidity, and carbon dioxide (CO<sub>2</sub>) concentration [16]. Samples were heated to 525°C at a rate of 10°C/min and were then held at 525°C for 1 minute before cooling to room temperature. Monitoring of the ambient air began before the oil was inserted into the test chamber. Air samples were also retrieved from the chamber for subsequent analysis by gas chromatography/mass spectrometry (GC/MS).

Van Netten *et al.* [14] noted that Mobil Jet Oil 254 (Exxon Mobile Corp., Fairfax, VA) was initially dark blue in color at room temperature. White smoke began to form when the hot plate reached approximately 275°C and the oil turned a dark brown-orange color. Charring of the oil began at 400°C while white smoke continued to form. At 500°C, only some charred material remained on the oil sample holder. Gas concentrations of 102.5 ppm CO and 460 ppm CO<sub>2</sub> were detected at 525°C [13]. Air sample results from GC/MS analysis indicated the presence of TCP isomers as well as volatile derivatives of pentane, hexane, and octane.

Castrol 5000 jet engine oil (BP North America, Parsippany, NJ) was initially orange in color and this lubricant began producing white smoke at approximately 285°C. Darkening of the oil began at 310°C, charring was observed at 350°C and only charred brown material remained at the end of thermal degradation. The CO<sub>2</sub> sensor measured a peak of 510 ppm CO<sub>2</sub> while the CO sensor detected a maximum of 140 ppm CO during degradation of the Castrol 5000 [16].

Van Netten *et al.* [14] noted that Exxon Turbo Oil 2380 (Exxon Mobile Corp., Fairfax, VA) began producing white smoke at about 275°C and darkening of the lubricant began at 300°C. Charring was observed at 310°C. At the end of the experiment only charred brown material remained. The CO<sub>2</sub> sensor measured a peak of about 510 ppm CO<sub>2</sub> and the CO sensor measured a peak of approximately 120 ppm CO [16].

Crane *et al.* [17] also evaluated Exxon Turbo Oil 2380. These researchers utilized a custom-built combustion chamber to heat the samples and analyze the evolved gases. The total volume of this chamber was only 12.6 L. Three milliliters of sample were placed in a semi-cylindrical quartz combustion boat located in a horizontal quartz tube furnace. The sample was continuously heated from room temperature until only charred material remained. Exxon 2380 began producing a measurable amount of CO at around 306°C when the authors also noted an increase in visible smoke production. At 344°C, the CO concentration was measured as 5,000 ppm. Only charred material remained when the temperature reached 350°C. The residual solid char continued to produce CO up to 530°C. Crane *et al.* found that as the thermal decomposition temperature increased, the production of CO began earlier and the maximum measured values of CO in the chamber increased. When Exxon Turbo Oil 2380 was thermally degraded at 600°C, the authors reported a much higher CO level of 17,000 ppm CO.

Bartl *et al.* [18] evaluated thermal degradation of pentaerythritol derivatives (the base component of jet engine oils) using thermogravimetric analysis (TGA) and differential thermal analysis (DTA). These researchers heated 10 mg of pentaerythritol from room temperature to 1000°C at

10°C/min in air. Figure 3 shows typical TGA and DTA data. The sample began to lose weight at approximately 275°C (which is roughly the temperature van Netten *et al* [14] began seeing visible smoke generation). The DTA data indicates sample heating due to exothermic reactions (i.e., burning) in the oil as the oil degrades. The first peak at approximately 350°C corresponds to a lower temperature oxidation reaction in which low molecular weight hydrocarbons were produced. The second higher temperature peak at about 570°C was likely due to oxidation of any remaining oil and charred products to CO and CO<sub>2</sub>. This can be roughly associated with the smoke, CO and CO<sub>2</sub> evolution at 525°C reported by van Netten *et al*[14].

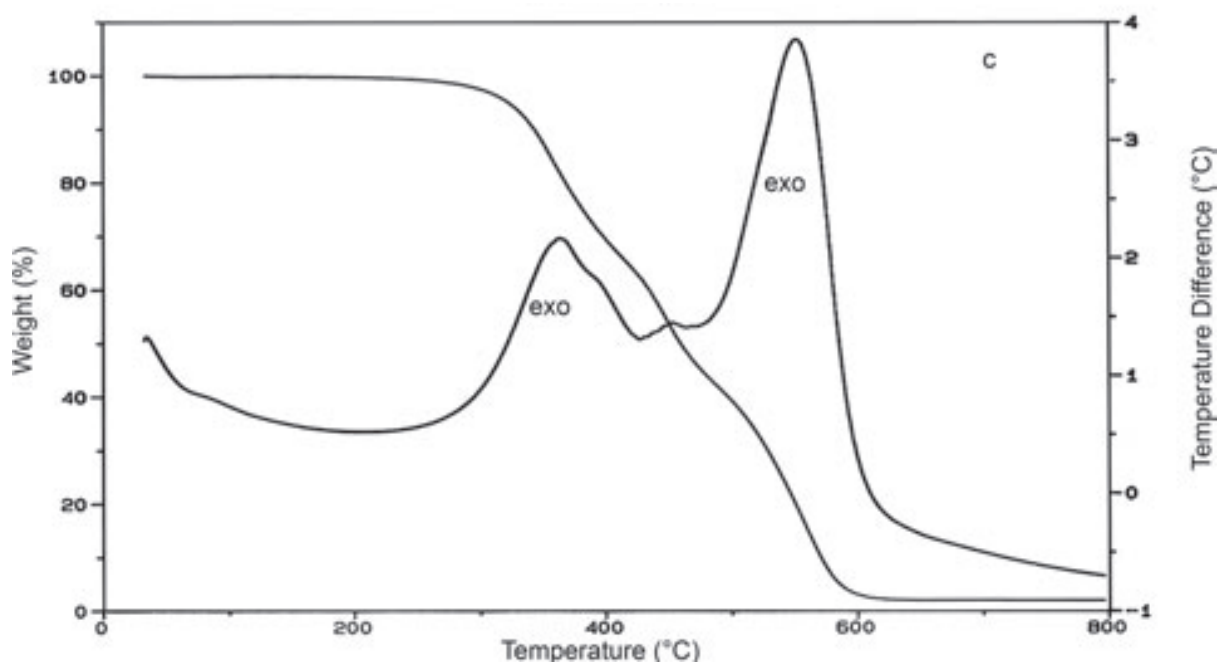


Figure 3. TGA and DTA plots of pentaerythritol derivative in air [17]. The low temperature exothermic peak at about 350°C corresponds to low temperature oxidation producing smoke, low molecular weight hydrocarbons, CO and CO<sub>2</sub>. The higher temperature exothermic peak corresponds to oxidation of the remaining oil and charred oil to smoke, CO and CO<sub>2</sub>.

### 2.3 Summary of Gaseous Contaminant Targets for Detection

Although Ref.[1] notes a wide range of gaseous contaminants of potential concern in aircraft including human bioeffluents (e.g., ethanol, acetone), cosmetics and perfumes (e.g., benzene, limonene, toluene, xylene, etc.) and dry cleaning agents (e.g., tetrachloroethene), the focus of this work is on those air contaminants that might arise from inadvertent malfunctions connected with the bleed air supplies from either the aircraft engine or the auxiliary power unit (APU). As noted

in Section 2.2 and summarized in Table II below, the principal contaminants of the aircraft bleed air supply could include (1) aerosolized droplets of jet engine or APU lubricating oil and (2) partially or fully pyrolyzed by-products of combustion of the working fluids. A number of approaches exist for monitoring of environmental air quality on aircraft to detect contamination of the bleed air supplies. Sensors could be located in either (i) the passenger cabin, (ii) along the bleed air supply path between the pre-cooler and the air conditioning packs, or (iii) between the air conditioning packs cooling the bleed air and the mixing chamber where the bleed air is mixed with the cabin recirculation air. The following section reviews the abilities of commercially available sensor technologies to detect these potential air contaminants.

**Table II**  
**Summary of Potential Bleed Air Contaminants**

<i>Potential Bleed Air Contamination Event</i>	<i>Probable Contaminant</i>
Engine oil leak producing aerosolized droplets of oil	<ul style="list-style-type: none"> <li>• Very fine mist of engine oil aerosols</li> </ul>
Partially pyrolyzed jet engine oil	<ul style="list-style-type: none"> <li>• Very fine mist of engine oil aerosols</li> <li>• Small amounts of carbon monoxide (CO) and carbon dioxide (CO<sub>2</sub>)</li> <li>• Misc. unburned hydrocarbons</li> <li>• Ultrafine smoke particles</li> </ul>
Fully pyrolyzed jet engine oil	<ul style="list-style-type: none"> <li>• Carbon monoxide (CO)</li> <li>• Carbon dioxide (CO<sub>2</sub>)</li> <li>• Ultrafine smoke particles</li> </ul>

## 2.4 Review of Commercial Gas Sensing Technologies

A rapidly increasing body of literature exists concerning environmental gas sensors that generate electrical signals (i.e., voltages or currents) in response to the presence of a contaminating analyte in air. Typical contaminants of interest include CO<sub>2</sub> in the air supplies of office buildings, CO from the exhaust of combustion processes in garages and other enclosed spaces and a wide variety of process gases in numerous industrial applications. Scientists and engineers worldwide are searching for ways to improve the intrinsic responses of the basic sensing materials. However, commercial sensor systems contain not only the discrete sensor element itself, but also the various technologies needed to transport the gaseous contaminant to the sensing material as well as the required electronics needed to supply power plus acquire, condition and transmit the sensor signals. A brief review is presented below for commercially available air quality sensors that might be applicable to aircraft air quality sensing. This review does not include either very

advanced sensing technologies that have yet to demonstrate significant market acceptance (and corresponding user experience) or expensive and labor intensive laboratory-class sensing techniques that would not likely find acceptance for routine aircraft operations.

*Catalytic-bead sensors* have been used commercially for many years to detect the presence of combustible gases. Early devices used a heated platinum wire to initiate combustion of the gas to be detected. The sensor electronics compared the resulting resistivity increase in the sensing platinum wire (due to increased temperature from combustion) to a reference wire that had been treated to prevent combustion. The sensor wire and the reference wire were connected in a Wheatstone bridge circuit to facilitate comparison. Sensor response to the target gas is enhanced in modern designs that utilize specially formulated catalyst containing porous beads around the heated platinum wires [19]. A schematic of a catalytic bead sensor is shown in Figure 4(a). Unfortunately, high operating temperatures are required for catalytic sensors and the devices are not particularly selective in their response to various combustible gases [20].

*Metal-oxide semiconductor (MOS) sensors* rely upon ionic absorption of the analyte's gaseous molecules to induce either a current or a voltage in the sensor material. See Figure 4(b). Two fundamental types of metal-oxide conductivity sensors exist: (1) n-type (e.g., tin oxide or zinc oxide) that, after reaching equilibrium with the oxygen in the air, react with reducing gases like CO to release electrons and increase the conductivity of the oxide and (2) p-type (e.g., nickel oxide or cobalt oxide) that react with oxidizing gases like O<sub>2</sub>, NO<sub>2</sub> or O<sub>3</sub> to consume electrons -- producing holes (i.e., charge carriers) and also increase the conductivity of the oxide [22]. Selectivity of the sensor to specific gases of interest can be improved by careful selection of the sensor alloy dopant, the operating temperature of the sensor material and gas filtration techniques [22]. Unfortunately, like catalytic bead sensors, high operating temperatures are also required for solid-state sensors.

*Electrochemical sensors* can be designed as either current generating (amperometric) or voltage generating (potentiometric) in response to the presence of the gas constituent to be measured [23-25]. In the case of a potentiometric sensor, the gas of interest establishes an electrochemical potential, which generates an open circuit voltage relative to a reference electrode. In the case of an amperometric sensor, as shown in Figure 4(c), a reducing (or oxidizing) gas of interest is oxidized (or reduced) at the working electrode. The magnitude of the current generated by this oxidation (or reduction) reaction is related to the concentration of the gas of interest. Solid polymer electrolytes emerged in the middle 1970s to alleviate some of the maintenance issues associated with aqueous electrolyte solutions [23]. In addition, ceramic oxide electrolytes are being investigated for monitoring the gaseous by-products of combustion [24,25].

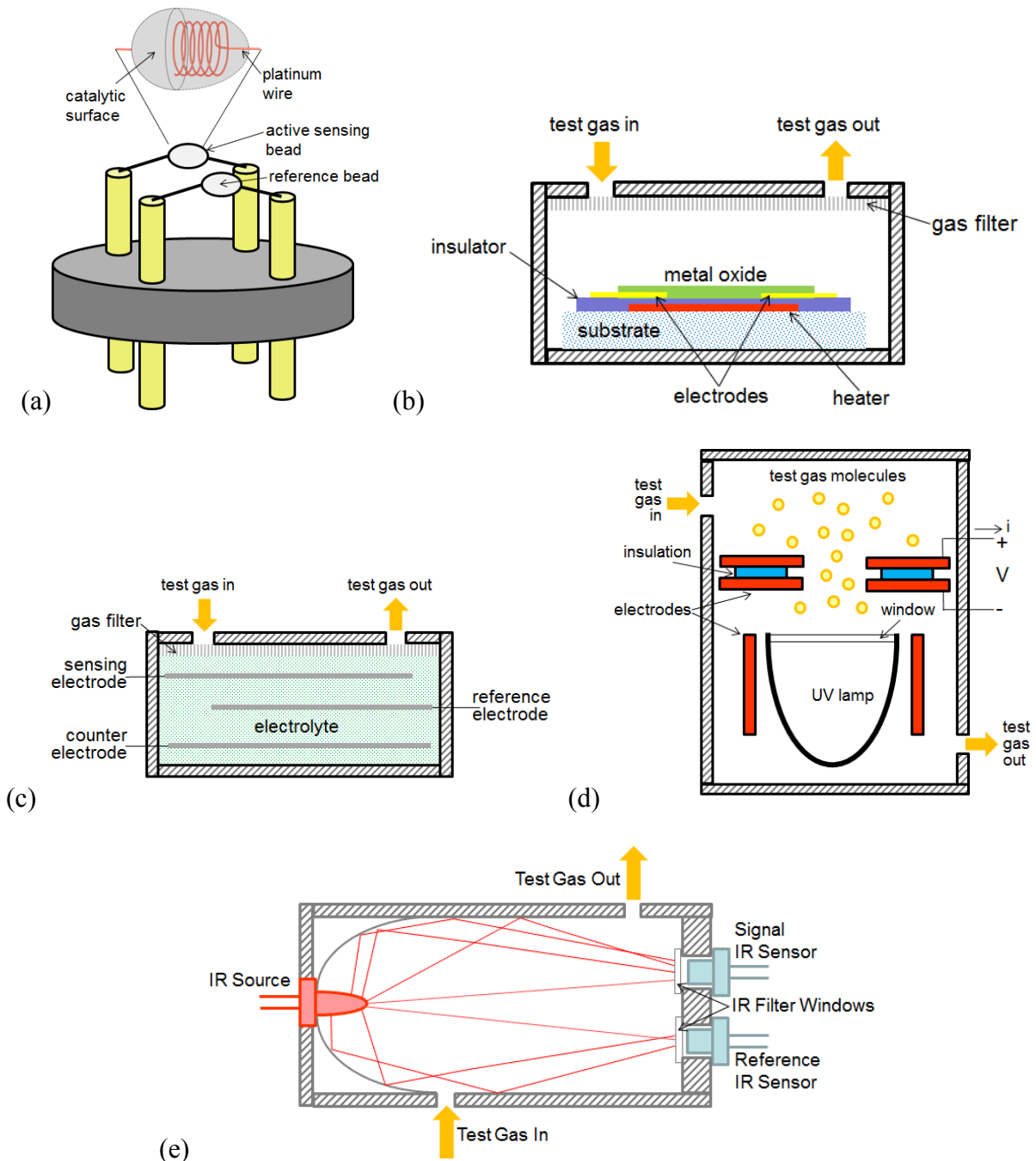


Figure 4. Schematic representation of commercial gas sensor detection technologies. (a) catalytic bead sensors typically used to detect inflammable gases; (b) conductometric sensors based upon metal-oxide semiconductor materials; (c) 3-electrode configuration of electrochemical sensors; (d) schematic representation of photoionization detectors for detecting volatile organic compounds like benzene, ethanol, acetone, amines and ammonia; and (e) two channel non-dispersive infra-red (NDIR) sensor often used for measuring CO<sub>2</sub> in HVAC systems. Schematics (a) and (d) adapted from [21]

As shown in Figure 4(d), *photoionization detectors* (PIDs) use light from an ultraviolet (UV) lamp to ionize gas molecules with ionization potentials less than the UV energy produced by the lamp [26]. Detector electrodes in PIDs are biased with a DC voltage and collect the free electrons from the ionized molecules. Detector current flows are thus proportional to the amount of the ionizing species. Many photoionization detector lamps use krypton gas in the UV lamp. Such lamps emit UV energy at 10.6 eV and can detect VOCs such as benzene, ethanol, acetone, amines, ammonia and aromatic compounds. The principal disadvantage of photoionization detectors resides sensor window cleanliness requirements for consistent performance.

Dedicated *infrared sensors* often use simple heated filaments to emit broadband IR radiation through the gas mixture of interest [21]. The radiation is then filtered to a narrow bandwidth IR beam for measurement by an IR sensor. Figure 4(e) shows one configuration that uses a single lamp, dual wavelength design where the second wavelength/detector combination monitors a wavelength expected to exhibit no absorption in air. This measurement is thus independent of the gas mixture and provides a reference signal for sensor compensation due to variations in lamp intensity and light scattering from particulates. The narrowly filtered bandwidth of these non-dispersive infrared (NDIR) sensors does not create complete spectral fingerprints of gases but instead enables measurement of the absorption of the narrow beam at a specific wavelength. According to Beers law, the amount of IR absorbed is proportional to the amount of the gas species in the detection pathlength. The actual wavelength can be selected and tuned to a specific and well-behaved IR absorption peak for a specific gas of interest. The principal disadvantages of NDIR sensors are in the sensitivity of the optical components to impact and vibration as well as maintenance of the cleanliness of the sensor windows for reliable operation.

NDIR sensors are finding increasing utilization in building HVAC systems to monitor levels of CO<sub>2</sub> in indoor air and modulate the intake of fresh outdoor air. This application is often referred to as Demand Controlled Ventilation and enables building owners to reduce the energy costs associated with over ventilating buildings during times of low occupancy. Commercial CO<sub>2</sub> sensors are available from a number of companies and Shrestha and Maxwell [27-30] investigated the abilities of commercial NDIR sensor systems to accurately and consistently evaluate the level of CO<sub>2</sub> under a range of environmental conditions including humidity, temperature and pressure. These researchers found wide performance variations among sensors of different manufacturers and sometimes even between identical sensor systems from the same manufacturer. Of particular concern was the automatic baseline adjustment algorithms incorporated in some sensor systems. This algorithm could introduce bias into the readings as the sensor systems attempts to automatically correct sensor readings to the expected value of 400 ppm CO<sub>2</sub> during the overnight periods of building vacancy. Shrestha and Maxwell note that NDIR CO<sub>2</sub> sensor systems should be individually calibrated prior to being placed into service. Periodic recalibrations would then appear to be warranted.

Table III summarizes the possible bleed air contaminants and the commercial sensor technology typically applied to detect and monitor the various contaminants in various non-aerospace applications.

**Table III**  
**Possible Bleed Air Contaminants and Potential Sensor Technologies**

---

<i>Possible Bleed Air Contaminant</i>	<i>Commercial Sensor Technology</i>
<ul style="list-style-type: none"><li>• Engine oil aerosols and</li><li>• Ultra-fine smoke particles</li></ul>	<ul style="list-style-type: none"><li>• Light scattering photoelectric detectors (aerosol/particle dia&gt;0.5 µm) or ionization detectors (aerosol/particle dia&lt;0.5 µm) depending upon the aerosol/particle size distribution</li></ul>
<ul style="list-style-type: none"><li>• Carbon Monoxide (CO)</li></ul>	<ul style="list-style-type: none"><li>• Electrochemical cell sensor with selectivity optimized for CO</li></ul>
<ul style="list-style-type: none"><li>• Carbon Dioxide (CO<sub>2</sub>)</li></ul>	<ul style="list-style-type: none"><li>• Non-dispersive Infrared (NDIR) sensor optimized for CO<sub>2</sub></li></ul>
<ul style="list-style-type: none"><li>• Misc. unburned hydrocarbons</li></ul>	<ul style="list-style-type: none"><li>• Photoionization detector depending upon the specific hydrocarbon(s) to be detected</li></ul>

---

### 3.0 Methods and Materials

#### 3.1 Evolved Gas Analysis by TGA/FTIR/MS

The Thermoanalytical Section of the NETZSCH Instruments Applications Laboratory (Burlington, MA) examined four common jet engine oil samples supplied by Auburn University. The temperature-dependent mass changes and evolved gases were analyzed using the NETZSCH TG 209 *F1 Iris*® thermogravimetric analyzer (TGA) coupled to a BRUKER Optics FTIR *SENSOR*™ and a NETZSCH QMS 403 *Aeolos* mass spectrometer [31]. A schematic of the experimental system is shown in Figure 5. The NETZSCH TG209*F1 Iris*® instrument can measure mass changes from 20°C to 1000°C with a resolution of 0.1µg. The heating rate is variable from 0.1 K/min and 100 K/min. The evolved gases were analyzed with a NETZSCH QMS 403 *Aeolos* system simultaneously coupled to the NETZSCH TG209*F1 Iris*® by means of a transfer line which was kept at a constant temperature of 250°C. The mass spectrometer of the QMS 403 allows detection of mass numbers between 1 and 300 amu. The evolved gas analysis was performed using the combined TGA-MS MSO-Windows analysis software package.

The oil samples and masses investigated were: BP Turbo Oil 274 (5.46 mg), BP Turbo Oil 2380 (5.01 mg), Aeroshell Turbine Oil 560 (5.65 mg) and Mobil Jet Oil II (5.22 mg). The samples were heated in platinum crucibles in air from room temperature to 650°C at 10°C/min.

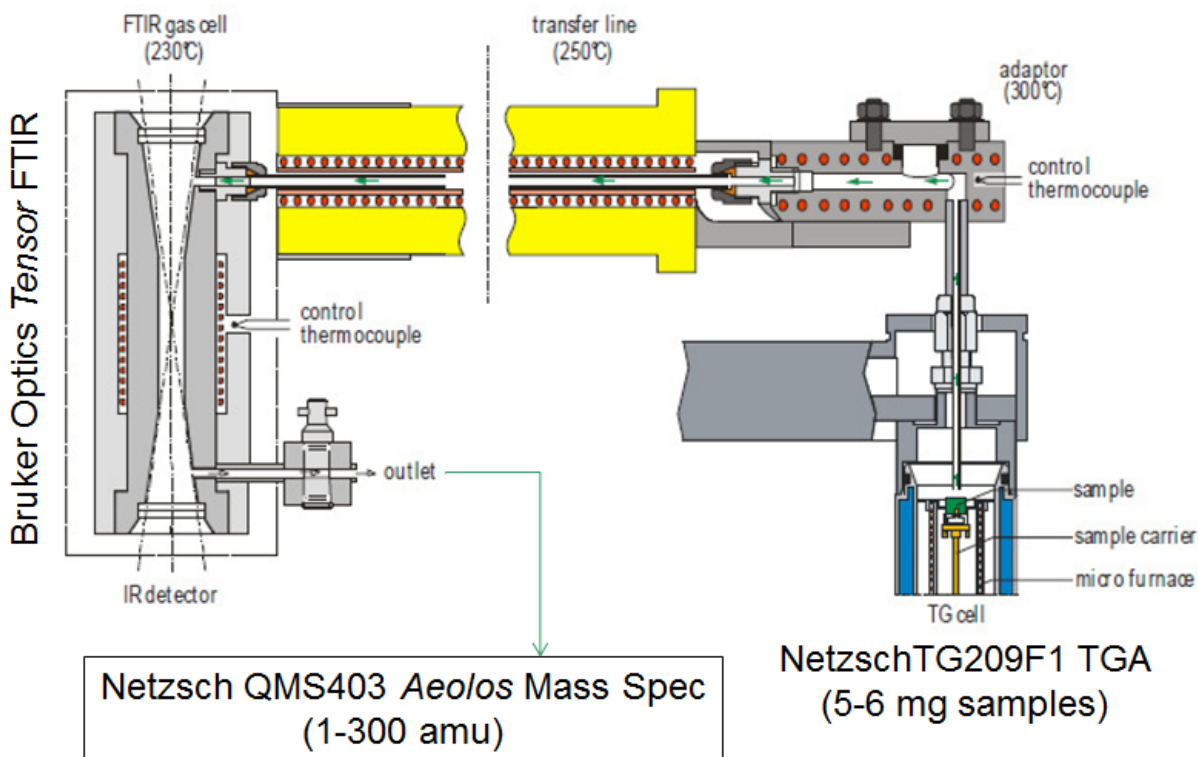


Figure 5. Evolved gas analysis experimental arrangement used by NETZSCH Instruments Applications Laboratory.

### 3.2 Steady State Testing of Commercial CO and CO<sub>2</sub> Sensors

The experimental setup utilized to simultaneously evaluate the steady state response of a large number of commercial CO and CO<sub>2</sub> sensor packages is shown in Figure 6.[32-34]

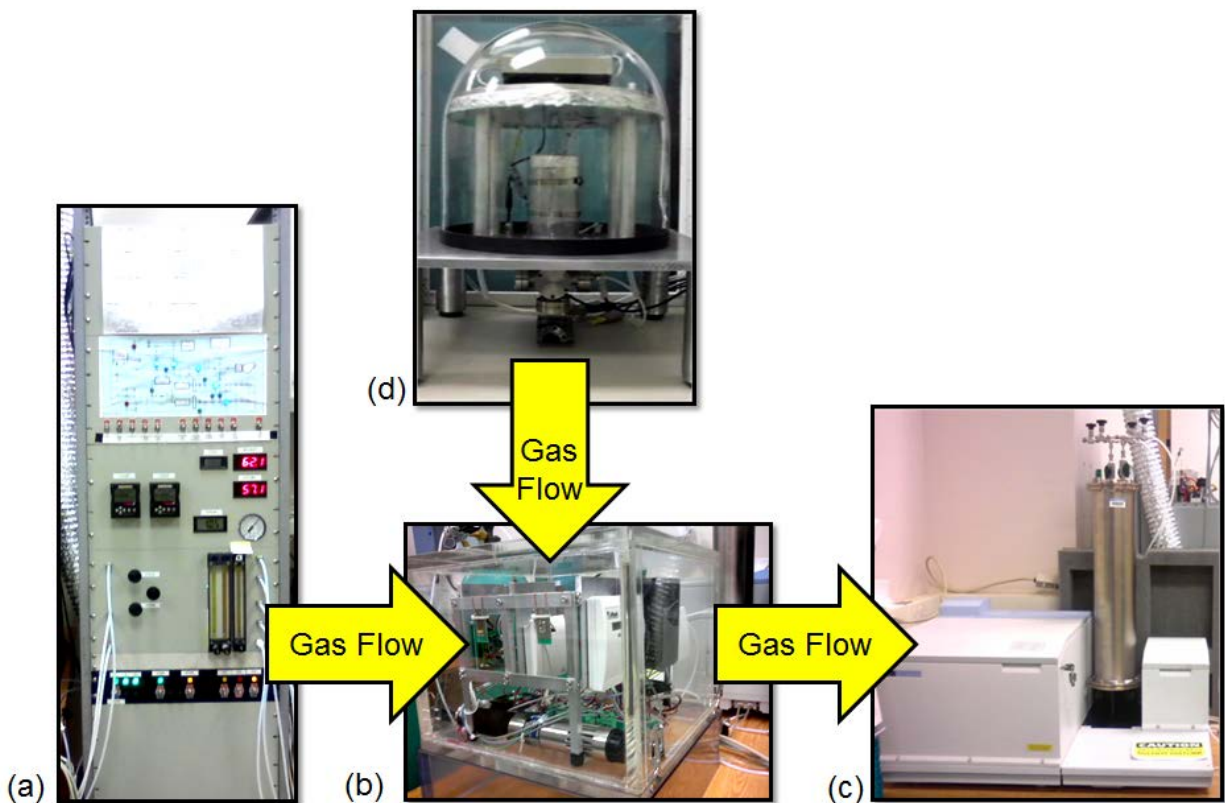


Figure 6. Experimental arrangement for testing of packaged commercial CO and CO<sub>2</sub> sensors.

The Calibration Gas Control Module is shown in Figure 6(a) and is responsible for the control of pressure, flow rates and mixing of carrying gases (typically nitrogen or nitrogen with 20% oxygen) as well as the contaminant test gases of interest (e.g., CO, CO<sub>2</sub>). The pressure setting within the system allows for testing of sensors at pressures representative of altitudes that are encountered in the airplane cabin environment. The gas lines in the system are rated for vacuum pressures of 15 inches of mercury (380 mm Hg) or about 50% of atmospheric pressure (50.5 kPa), which corresponds to altitudes up to 12,000 feet (3,700 meters). The flow meters allow precise control of the gases and allow custom mixing ratios for sensor performance testing.

The Commercial Sensor Analysis Module shown in Figure 6(b) is an enclosed, vacuum-sealed, PMMA chamber, which has a total volume of 42.4 liters. With this module, an environment replicating the low pressure airplane cabin can be maintained to test commercial sensor performance in regards to detection of the gases of interest.

The Oil Degradation Module, shown in Figure 6(d), includes a microbalance from which 1g oil samples were suspended into a cylindrical heater. The Scientech SM124D (Boulder, CO) microbalance measured the mass of the sample within  $\pm 0.6$  mg over the experimental mass range. The temperature of the oil sample was measured within  $\pm 2^\circ\text{C}$  over the experimental temperature range (room temperature to  $600^\circ\text{C}$ ). The Watlow ceramic fiber heater (Chicago, IL) has a operating range up to  $2200^\circ\text{C}$ . The microbalance-heater assembly was encapsulated by a 50 L bell jar to contain the evolved gases. Room temperature air from outside the bell jar was provided within the upper region of the bell jar (adjacent to the microbalance) by two plastic tubes, approximately 12 mm in diameter. The supply outside air was forced through a 12 mm hole below the balance and down through the heater past the hanging crucible assembly. In addition, a vacuum pump connected to the FTIR pulled the air from the bell jar, at a rate of 11,600 sccm via a tube that connects both the sensor chamber and the FTIR to the thermal degradation system. See Figure 6(c). This prevented any evolved gases from migrating into the top of the bell jar and affecting the performance of the microbalance. The thermal degradation system was enclosed by a custom built fume hood to contain any possible leaks in the system. Once the evolved gases passed through the sensor chamber and the FTIR, they were removed by the building exhaust.

The FTIR Gas Analysis Module shown in Figure 6(c) was used as the standard to verify the gas composition of various concentrations of test gases used for evaluating sensor performance. This module contained a Spectrum GX FTIR System (Perkin Elmer, Shelton, CT, USA), as well as an M-5-22-V variable pathlength long-path gas cell (Infrared Analysis, Inc., Anaheim, CA, USA). The optical path is folded in a total volume of 8.5 liters, while the cell path length was held constant at 2.24 m. The analyzed wavenumber range typically varied from  $600\text{ cm}^{-1}$  to  $4000\text{ cm}^{-1}$  with a spectral resolution of  $0.5\text{ cm}^{-1}$ . The IR source was produced by a temperature stabilized wire coil that operates at 1350 K. The material for the cell windows in the variable pathlength long pass gas cell was potassium chloride (KCl) and 4 mm thick. The detector for the IR beam was a fast recovery deuterated triglycine sulfate (FR-DTGC) module.

### 3.3 Transient Testing of Commercial CO Sensors

The accuracy, repeatability and transient performance of the following discrete CO sensors were evaluated: (i) Alphasense CO-B4, (ii) Figaro TGS5042 and (iii) e2v EC4-500-CO.[35] These devices are shown in Figure 7.

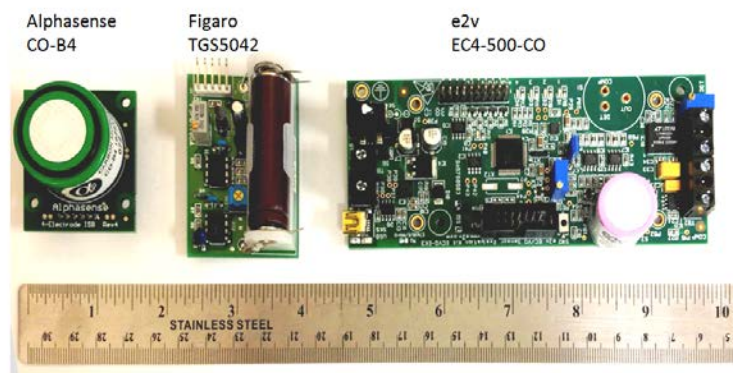


Figure 7. CO sensors and evaluation boards investigated in this work: Alphasense CO-B4, Figaro TGS5042 and e2v EC4-500-CO

The transient response of each CO sensor to an “instantaneous” change in CO concentration was evaluated using a test chamber with a total volume of 16.7 L. The experimental procedures allowed the temporal response of each sensor to be evaluated by exposing each sensor to an almost “instantaneous” step function concentration change. A certified test gas was supplied from pre-mixed tanks of specified concentrations of CO (balance of nitrogen) to pressurize a thin membrane bladder inside the test chamber as shown in Figure 8. A pressure transducer was used to monitor the gas pressure inside the inflatable bladder. The thin membrane bladder was used to contain the gas until the bladder was mechanically burst and the test gas released into the test chamber. Mixing in the chamber was ensured by a fan at the top of the chamber. A sharp tool was inserted through a small temporary opening in the chamber to burst the bladder. A rubber stopper was then quickly placed into the opening to seal the chamber for the duration of the test. A metal screen was mounted at the bottom of the chamber between the inflatable bladder and the sensors to prevent the bursting of the bladder from damaging any of the sensors. Ball valves were used to isolate the chamber during testing and, once a test was completed, clean laboratory air was used to purge the chamber into the building exhaust system.

The step-function change in imposed gas concentration and the expected sensor response are shown schematically in Figure 9.

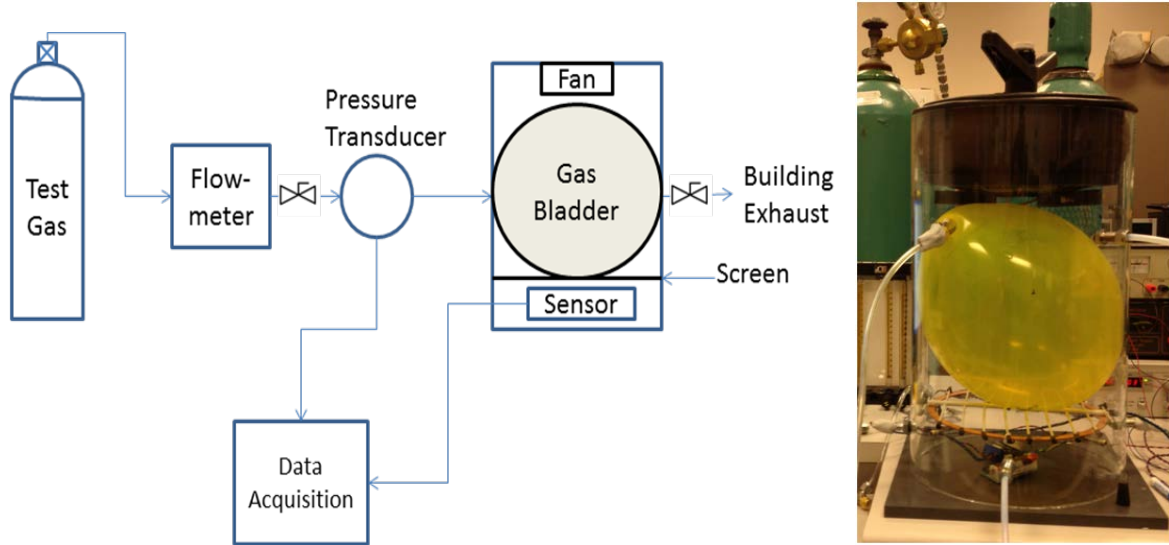


Figure 8. Schematic and picture of the experimental arrangement for transient testing of commercial CO sensors.

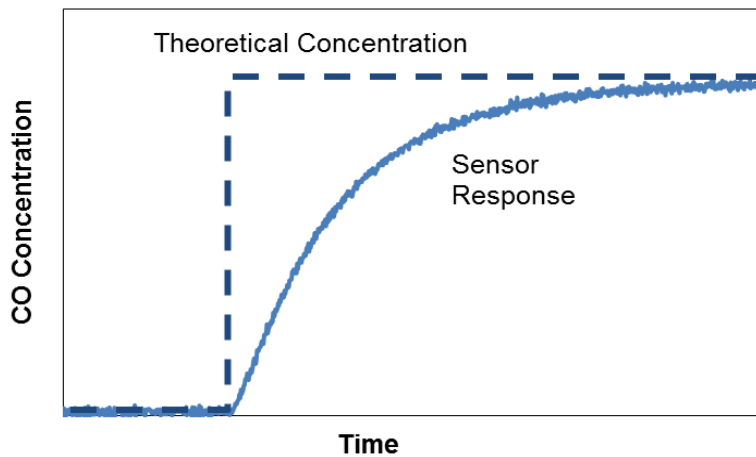


Figure 9. Schematic of the desired instantaneous gas concentration profile (dashed line) compared with an expected sensor response (solid line)

### 3.4 Transient Testing of Commercial CO<sub>2</sub> Sensors

The accuracy, repeatability and transient performance of the following discrete CO<sub>2</sub> sensors were evaluated: (i) Madur madIR-D01, (ii) E2V IR11EJ and (iii) Figaro K30.[36] These devices are shown in Figure 10. In some commercial CO<sub>2</sub> sensor designs, the sensor incorporates a micropump to move the sample gas directly through ports into the sensing chamber. The Madur madIR-D01 CO<sub>2</sub> sensor utilizes this design. In other sensor designs, the gas sample is allowed to slowly diffuse through a dust filter into the sensing chamber and is not actively pumped. The E2V IR11EJ sensor is of this type and the manufacturer provides a gassing hood to flow gas over

the sensor. The gas is then allowed to diffuse into the NDIR test area. The Figaro K30 sensor design allows either method to be used.

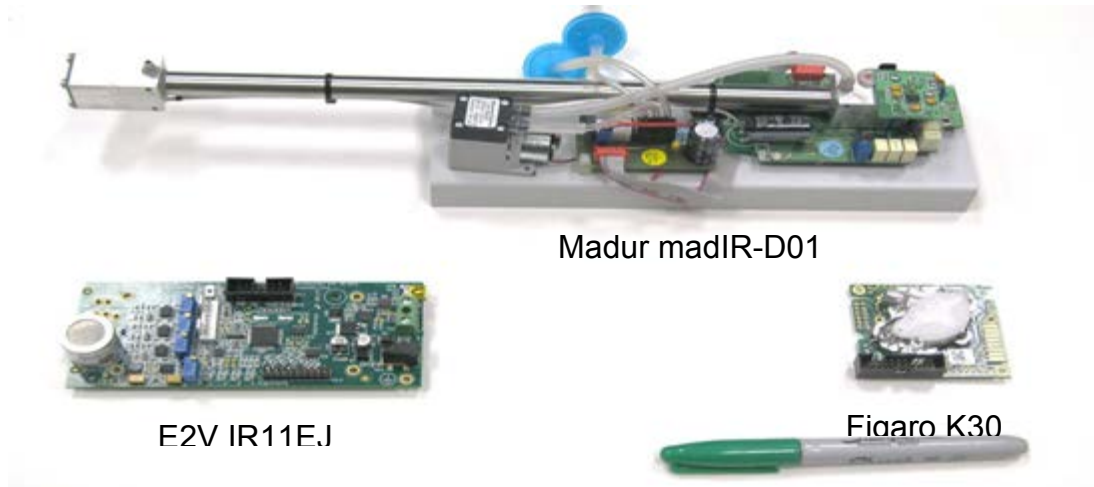


Figure 10. CO<sub>2</sub> sensors and evaluation boards investigated: Madur madIR-DO1 CO<sub>2</sub>, E2V IR11EJ, Figaro K30

Figure 11(a) shows a schematic of the overall testing apparatus used to perform the transient tests. The membrane burst apparatus described in Section 3.3 was modified to enable the test gas in the membrane burst chamber to be directly supplied from the chamber by a micropump to the externally located sensor being evaluated. Since the readings of an NDIR sensor can be affected by absolute pressure, a pressure transducer was included to ensure that the gas flow rates achieved by the micropump did not pressurize the sensor system. The flow rate used completely exchanged the gas in the gassing hood seven times per second. Note also that a baffle (Figure 11b) was added to the gassing hood of the E2V IR11EJ sensor to maximize test gas entry into the active sensor area. The sensor responses were also compensated for temperature effects.

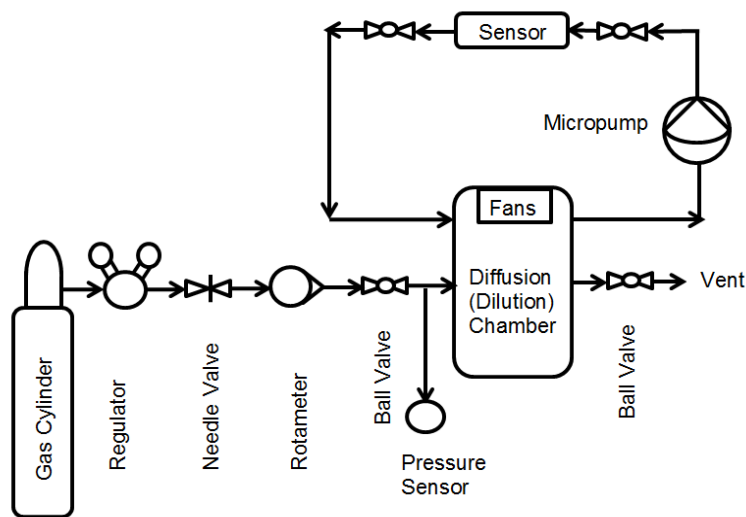


Figure 11. Overall arrangement of the experimental apparatus for transient testing of discrete commercial CO<sub>2</sub> sensors.

## 4.0 Results and Discussion

### 4.1 Characterization of Fumes from Oil Degradation Experiments

Figure 12 shows the change in BP Turbo Oil 274 sample mass as a percentage of the total (TG) and the mass change rate (DTG) as the sample heated from room temperature to 650°C. In addition the Gram-Schmidt reduced data set shows essentially the total integrated intensity of the FTIR spectra and peaks or shoulders in the Gram-Schmidt curve can be interpreted as the appearance of new species in the evolved gas mixture. The TG data show mass loss beginning around 200°C with the rate of maximum mass loss occurring at 300.2°C (DTG). The peak in gas evolution is shown to occur at 300.8°C in the Gram-Schmidt data in close agreement with the sample mass loss data.

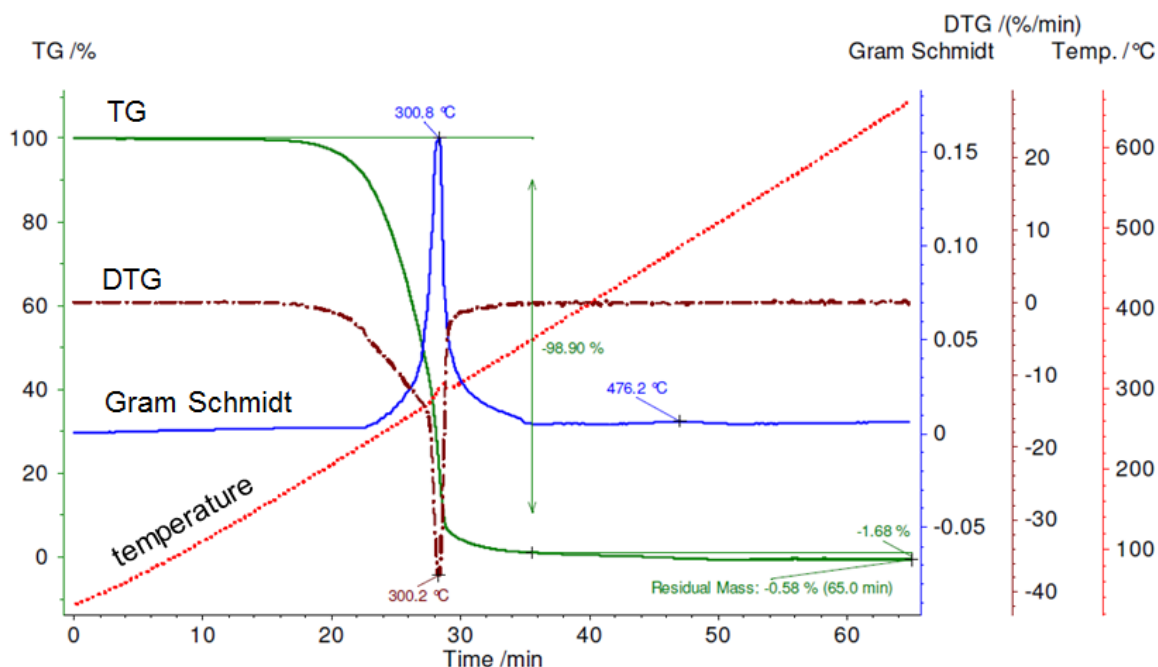


Figure 12. Mass changes of BP274 oil sample as a function of exposure temperature.  
 Sample size = 5.46 mg and 10°C/min heating rate in air.  
 (TG=mass change, DTG=mass change rate)

The BP Turbo Oil 274 mass spectrometry ion-current curves for H<sub>2</sub> (2 amu), H<sub>2</sub>O (17; 18 amu) and CO<sub>2</sub> (12; 44 amu) are plotted in Figure 13(a) along with the already analyzed TG data. All the species evolve as a sharp peak at 293.5°C. Figure 10(b) shows the mass spectrometry ion-current curves for C<sub>2</sub>H<sub>5</sub> (29 amu), C<sub>2</sub>H<sub>6</sub> (30 amu), CH<sub>2</sub>OH (31 amu), CH<sub>3</sub>OH (32 amu), H<sub>2</sub>S (34 amu), C<sub>3</sub>H<sub>3</sub> (39 amu) and C<sub>3</sub>H<sub>7</sub> (43 amu) along with the already analyzed TG data. C<sub>2</sub>H<sub>6</sub>, C<sub>3</sub>H<sub>3</sub> and C<sub>3</sub>H<sub>7</sub> evolve as a sharp peak at 293.5°C, while the signals for all the other fragments and molecules show a broad asymmetric peak.

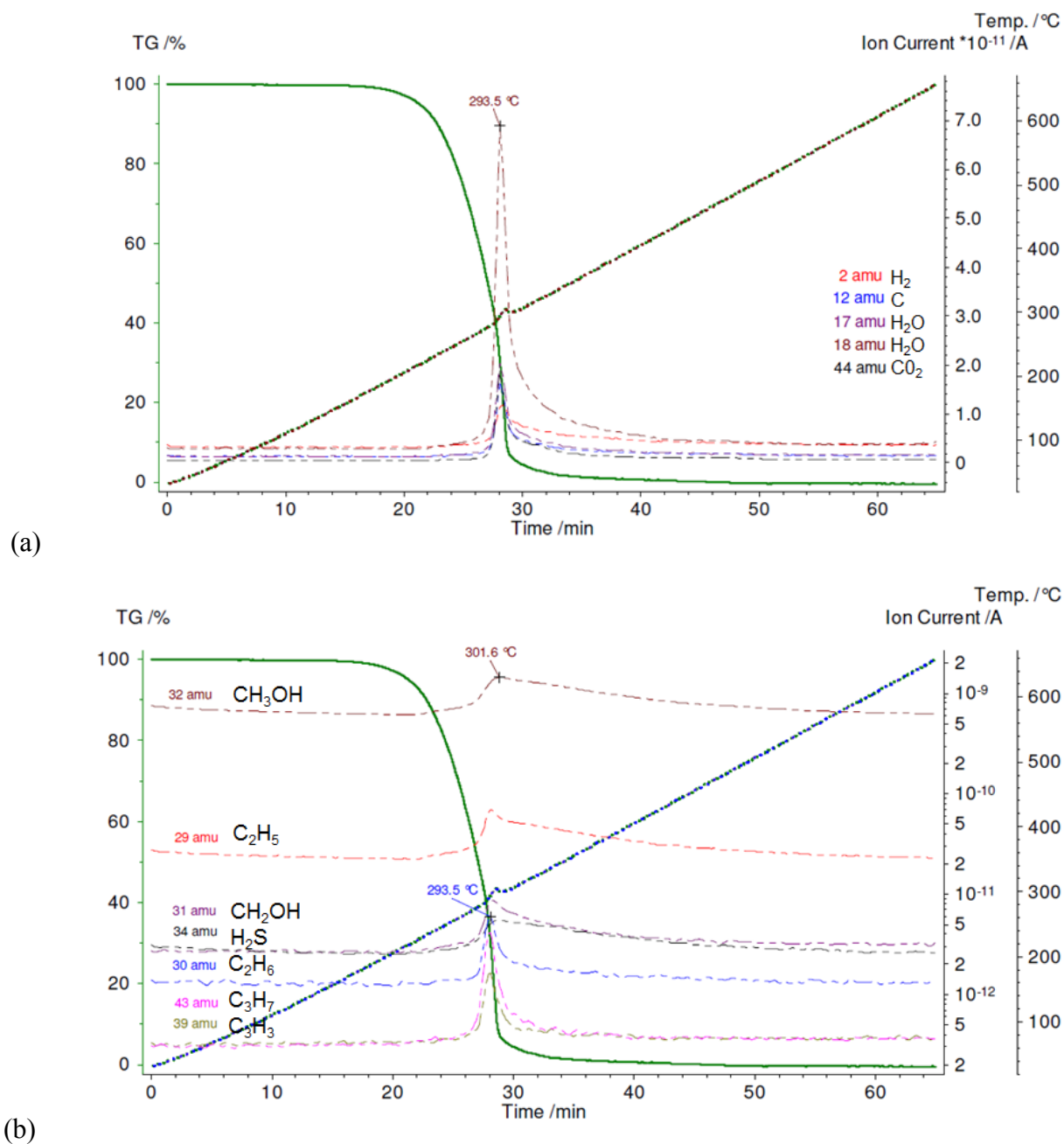


Figure 13. Time dependent mass loss and sample temperature data shown with mass spectrometry ion-currents for the following evolved gaseous species: (a) 2 amu – H<sub>2</sub>, 12 amu - C, 17 and 18 amu – H<sub>2</sub>O, 44 amu – CO<sub>2</sub>; (b) 32 amu – CH<sub>3</sub>OH, 29 amu – C<sub>2</sub>H<sub>5</sub>, 31 amu – CH<sub>2</sub>OH, 34 amu – H<sub>2</sub>S, 30 amu – C<sub>2</sub>H<sub>6</sub>, 43 amu – C<sub>3</sub>H<sub>7</sub>, and 39 amu – C<sub>3</sub>H<sub>3</sub>.

Additional experiments with BP Turbo Oil 2380, Aeroshell Turbine Oil 560 and Mobil Jet Oil II yielded similar results for peak degradation temperatures and evolved gases. The peak degradation temperatures are summarized in Table IV and show that all the oils exhibited the greatest mass losses at temperatures ranging from 301-326 °C.

**Table IV**  
**Jet Engine Oils: Peak Degradation Temperatures**

<i>Jet Engine Oil</i>	<i>Peak Degradation Temperature</i>
BP Turbo Oil 274	301 °C
BP Turbo Oil 2380	305 °C
Aeroshell Turbine Oil 560	326 °C
Mobil Jet Oil II	307 °C

A 3-D plot of FTIR spectra vs. time for the BP Turbo Oil 274 sample is shown in Figure 14. The FTIR spectra clearly show the peak evolution of various hydrocarbons and CO<sub>2</sub> occurs at about 28 minutes in agreement with the mass loss results shown in Figure 12(a).

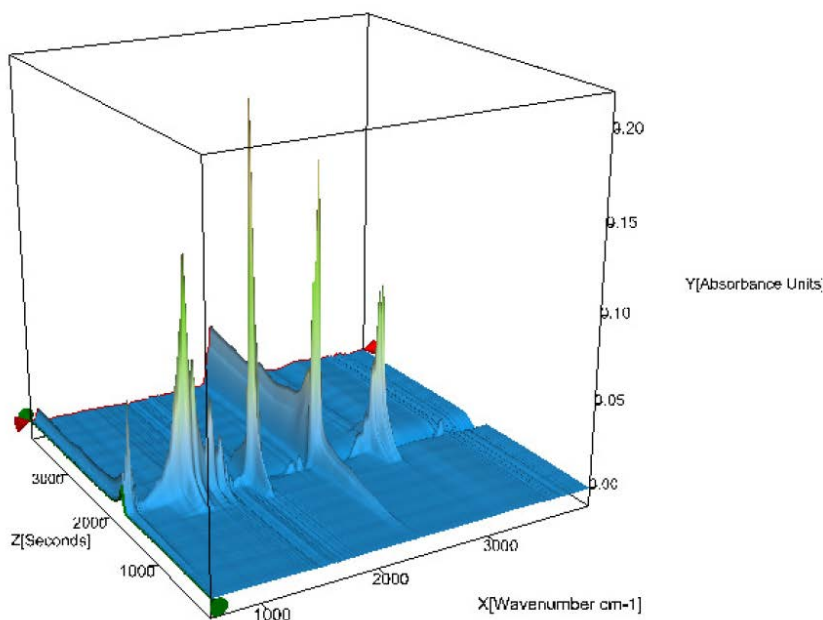


Figure 14. 3D plot of gas evolution FTIR absorbance data versus time for BP274 sample.

The FTIR spectra obtained at the time of greatest mass loss for each of the four oils investigated are shown in Figure 15(a). Each of the oils exhibited similar peaks with minor differences in relative peak heights amongst the four jet engine oils investigated. Principal components analysis was performed on the experimental FTIR data to determine the number of components most likely present in the evolved gas species from the heated engine oil samples. These results were then compared to the mass spectrometry data for verification and to determine the probable identity of the gaseous components being evolved during thermal degradation.

Figure 15(b) shows pure component spectra from the following possible constituents of the evolving gaseous mixture: methanol, formaldehyde, carbon monoxide, carbon dioxide and water. Note the strong and well identifiable  $\text{CO}_2$  peak between wavenumbers of  $2300\text{-}2400\text{ cm}^{-1}$ . There is no overlap between this peak and other possible species.  $\text{CO}_2$  exhibits another peak between wavenumbers of  $600\text{-}700\text{ cm}^{-1}$ . CO exhibits FTIR absorbance peaks between wavenumbers of  $2050\text{-}2250\text{ cm}^{-1}$  with minimal overlap from other possible species. Peaks for methanol ( $\text{CH}_4\text{O}$ ) appear at  $2800\text{-}3050\text{ cm}^{-1}$  as well as  $1000\text{-}1100\text{ cm}^{-1}$ . Formaldehyde ( $\text{CH}_2\text{O}$ ) absorption peaks occur from  $2700\text{-}3000\text{ cm}^{-1}$  and also from  $1700\text{-}1800\text{ cm}^{-1}$ . Water is a strong IR absorber over a wide range of wavenumbers from  $1400\text{-}2000\text{ cm}^{-1}$  as well as  $3500\text{-}3950\text{ cm}^{-1}$ . Overlap of the absorption peaks due to water and methanol with formaldehyde's absorption peaks complicates evolved gas analysis when these three species may all be simultaneously present.

Principal components analysis was also applied to the FTIR spectra of gases evolved as a function of time for BP Turbo Oil 2380 thermally degraded in the Oil Degradation Module shown in Figure 6(d). Initial calculations utilized simulation data sets created from pure component database spectra for comparison against the evolving gas mixtures. After using principal components regression analysis to determine likely concentrations for methanol ( $\text{CH}_4\text{O}$ ), formaldehyde ( $\text{CH}_2\text{O}$ ), carbon dioxide ( $\text{CO}_2$ ), carbon monoxide (CO) and water vapor ( $\text{H}_2\text{O}$ ) of the BP Turbo Oil 2380 time evolved samples, reconstructed prediction FTIR spectra were calculated. These reconstructed spectra were then compared to the experimentally obtained FTIR data as shown in Figure 16(a-d) for elapsed times of 10 min., 30 min., 60 min. and 90 min. The RMSE between the predicted and actual spectra for each of the time-evolved spectra were calculated to be 2.7%, 8.4%, 9.2%, and 9.0% for 10 min., 30 min., 60min., and 90 min., respectively. The average RMSE between the predicted and actual spectra for all 20 of the time evolved spectra was found to be 7.5%. The principal components analysis indicated that the following species were present in varying amounts: water vapor ( $\text{H}_2\text{O}$ ), methanol ( $\text{CH}_4\text{O}$ ), carbon monoxide (CO), carbon dioxide ( $\text{CO}_2$ ) and perhaps formaldehyde ( $\text{CH}_2\text{O}$ ) [32].

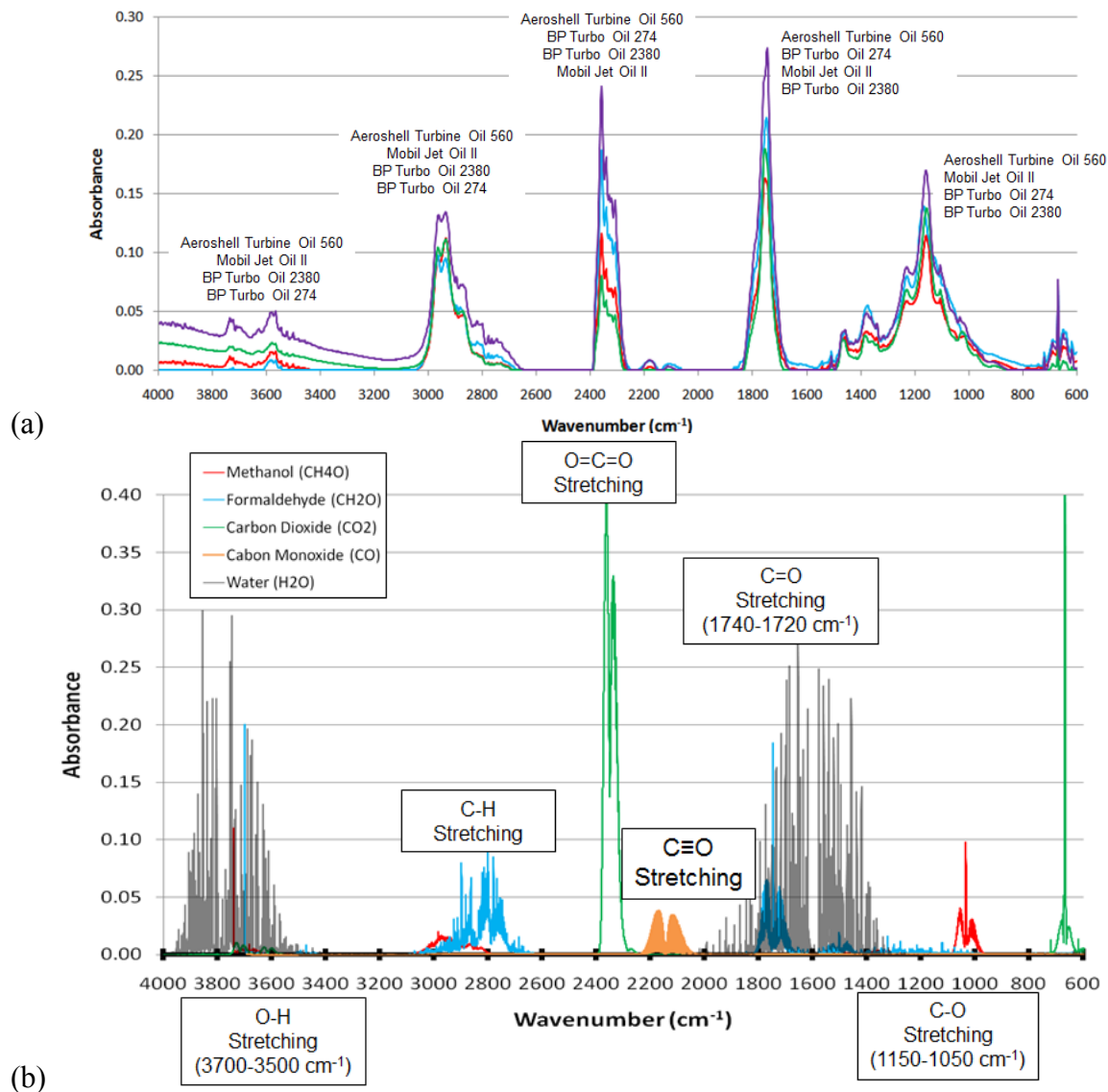


Figure 15. (a) FTIR scans of BP Turbo Oil 274(301°C), BP Turbo Oil 2380(305°C), Aeroshell Turbine Oil 560 (326°C) and Mobil Jet Oil II (307°C) at the indicated temperatures of greatest mass loss. The order of the data in each peak from each oil sample is indicated by the listing adjacent to the peak. (b) Pure theoretical spectra from various possible components of the evolving gas mixture. The infrared bond excitation regions are also indicated.

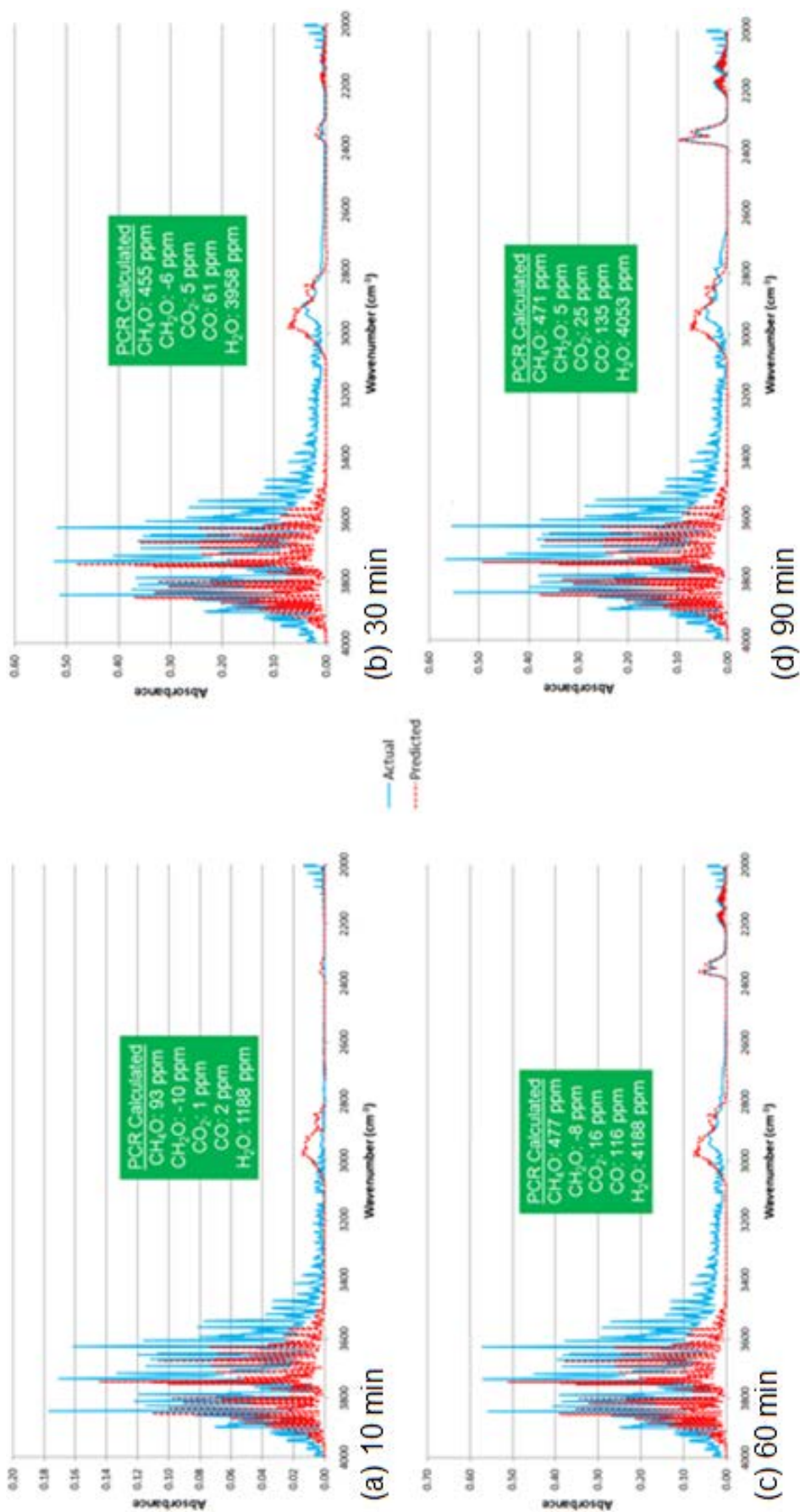


Figure 16. Experimental and calculated FTIR spectra and predicted evolved gas compositions at the times indicated during thermal degradation of BP Turbo Oil 2380. See the text for a discussion of the calculation procedures [32].

## 4.2 Commercial CO and CO<sub>2</sub> Sensor Response Characterization

As noted previously, NDIR-based commercial sensor technologies exist for detecting CO<sub>2</sub> in the air supplies of office buildings. In addition, electrochemically-based technologies are available for assessing the presence of CO from the exhaust of combustion processes. Commercial sensor systems contain all the various technologies needed to transport the test gas to the actual sensing element as well as the required electronics needed to supply system power plus acquire, condition and transmit the resultant sensor response signals. Sensor technologies developed for office buildings or garages cannot be applied to aircraft applications without being thoroughly vetted to ensure reliable performance in conditions representative of the aircraft application.

As reported below, the accuracy and precision (sensitivity and detection limits) as well as transient response characteristics for NDIR CO<sub>2</sub> sensors and electrochemical CO sensors have been investigated using premixed calibration gases over a range of pressures representative of aircraft operation.[32-36] In addition, typical CO<sub>2</sub> and CO sensor responses due to fumes generated from actual thermal degradation of jet engine oil are also presented.[32-34]

### 4.2.1 Steady State Responses to Calibration Gases

*4.2.1.1 Commercially packaged NDIR CO<sub>2</sub> sensors:* Many commercially available NDIR CO<sub>2</sub> sensor technologies utilize specialized drying techniques to remove water vapor from the air. Typical sensors exploit the 4.26 μm infrared absorption band (wavenumber = 2349 cm<sup>-1</sup>) of CO<sub>2</sub> for the measurement since that wavelength provides the least interference with the absorption bands of other gases. In addition, many commercial systems also utilize an automatic background calibration technique that presumably avoids having to actually calibrate the sensors. This method is reasonable for office buildings that are essentially unoccupied for long periods of time (e.g., overnight, weekends). Since CO<sub>2</sub> is generated by building occupants, the air in office buildings should refresh during extended unoccupied periods and return to the 400 ppm CO<sub>2</sub> level that is typical of the overall atmosphere. The electronics in sensors that attempt to exploit this 400 ppm night-time CO<sub>2</sub> level automatically adjusts the calibration of the sensor to this periodically measured low level of CO<sub>2</sub>. However, such “calibrations” could prove problematical for sensors on aircraft that do not experience such repetitive low levels of CO<sub>2</sub>.

Figure 17 shows a typical set of commercial NDIR CO<sub>2</sub> sensor responses as well as the FTIR measurement during exposure to a calibration test gas of nitrogen and carbon dioxide. The overall test chamber pressure was maintained at 0.67 atm (10,780 ft equivalent altitude) and 1340 ppm CO<sub>2</sub>. The responses of the sensors and the FTIR appear to track the slowly varying CO<sub>2</sub> level in the test chamber. Some sensors (A6 and A7) measured higher levels of CO<sub>2</sub> than the test gas composition (1340 ppm at 0.67 atm) while the other sensors indicated lower levels of CO<sub>2</sub> than expected. The FTIR measurement agreed most closely with the actual composition of the calibration test gas. Additional tests of these sensors indicated very repeatable responses over the range of pressures investigated. Laboratory recalibration of these NDIR sensors would likely enable very accurate and precise measurements of the calibration test gases.

The effect of pressure on sensor response was also investigated and typical results are shown in Figure 18. The theoretical pressure sensitivity of the CO<sub>2</sub> partial pressure for a gas composition of 1100 ppm CO<sub>2</sub> at 1 atmosphere (i.e., CO<sub>2</sub> partial pressure of 0.11 kPa) was calculated assuming ideal gas behavior. The theoretical dependence of CO<sub>2</sub> partial pressure upon chamber pressure (slope = -0.18) was then experimentally compared to sensor indications from a Johnson Controls CD-WA0 NDIR CO<sub>2</sub> sensor. As shown in Figure 18, the commercial sensor exhibited a higher sensitivity to pressure (slope = -0.24) than expected from the ideal gas law. Table V shows the pressure sensitivity of a number of additional NDIR CO<sub>2</sub> sensors investigated and all sensors exhibited higher sensitivity to pressure that expected. The average sensor was approximately 27% more sensitive to pressure than expected.

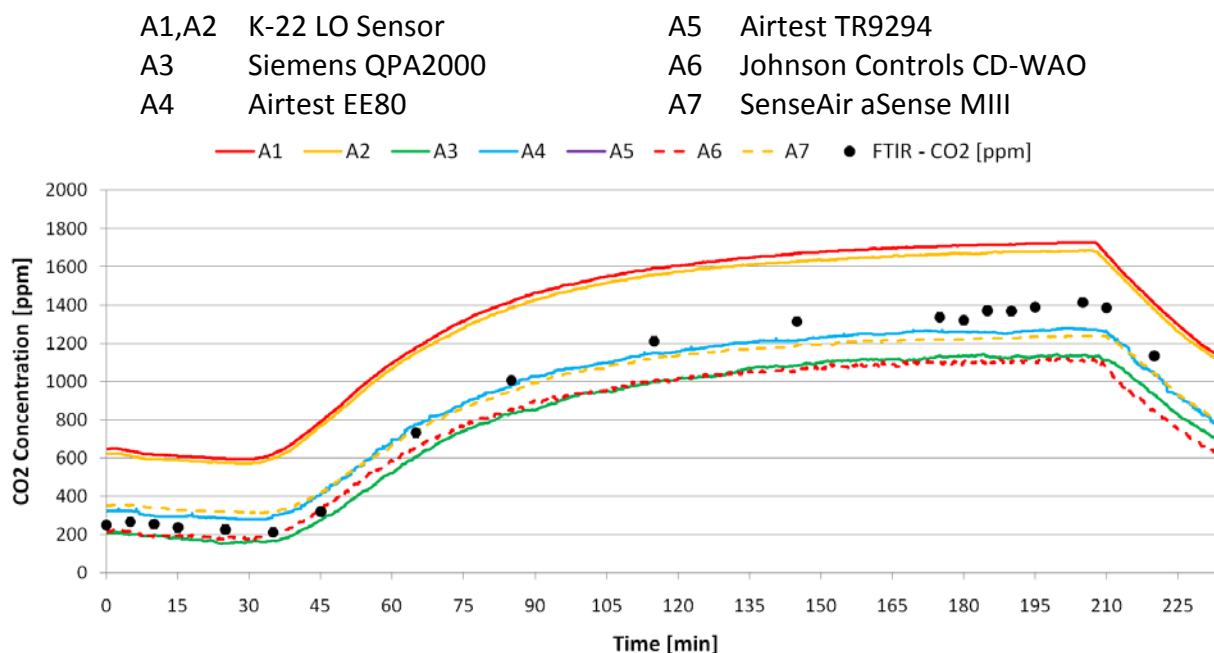


Figure 17. Laboratory FTIR and commercial CO<sub>2</sub> NDIR sensor responses to introduction of 1340 ppm CO<sub>2</sub> in nitrogen at 0.67 atm pressure in the test chamber (10,780 ft equivalent altitude). Indicated time is from the beginning of introduction of the test gas. Test gas flow stopped at 200 min.

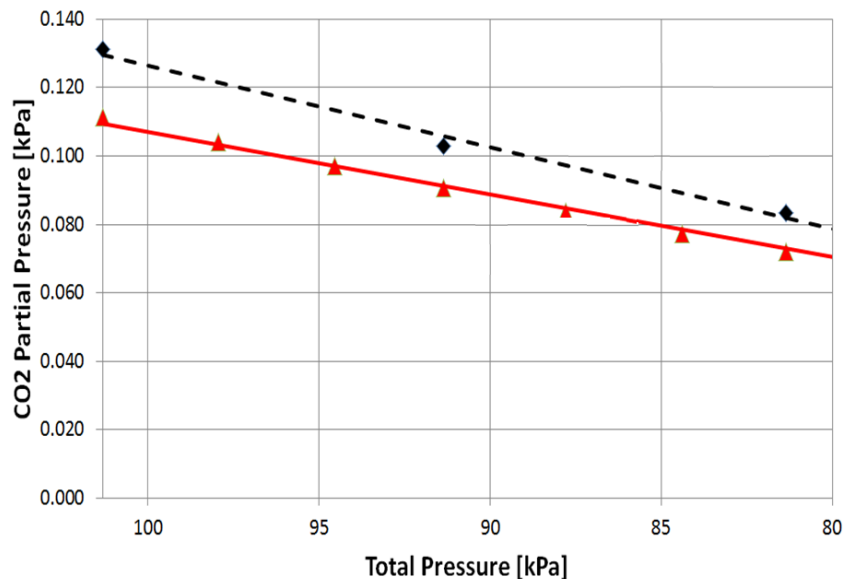
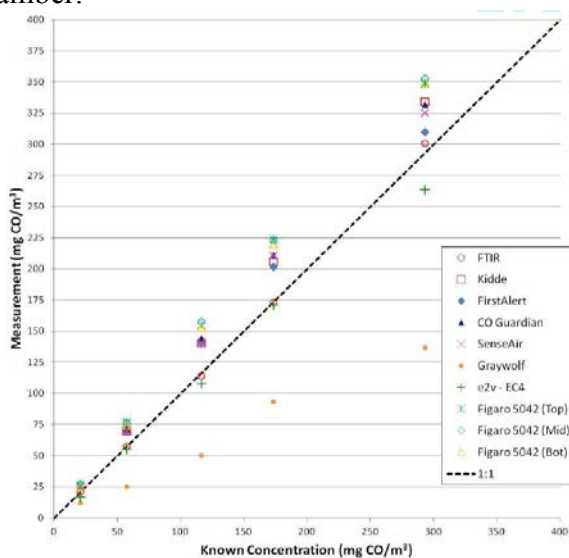


Figure 18. Theoretical pressure sensitivity (triangles) of the CO<sub>2</sub> partial pressure calculated assuming ideal gas behavior compared to sensor indications from a typical NDIR CO<sub>2</sub> sensor (diamonds: Johnson Controls CD-WA0). Note that the commercial sensor exhibits a higher sensitivity to pressure than expected from theoretical considerations.

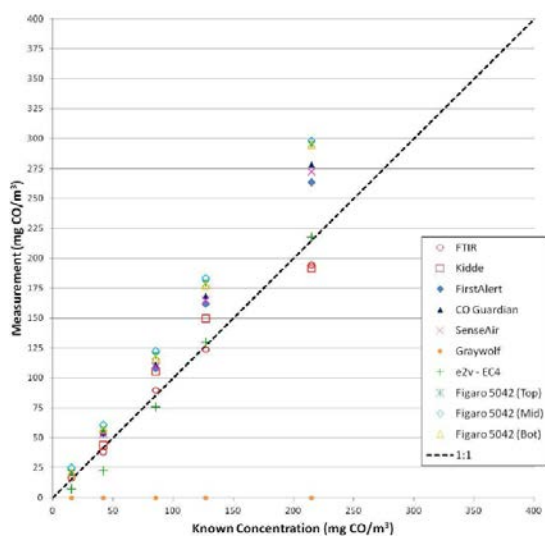
**Table V**  
**Pressure Sensitivity of Commercial NDIR CO<sub>2</sub> Sensor Packages**

<u>Sensor Manufacturer</u>	<u>Model Number</u>	<u>Theoretical Slope</u>	<u>Actual Slope</u>	<u>% Difference</u>
<b>Expected Pressure Dependence</b>		<b>-0.0018</b>		
AirTest Technologies	TR9290		-0.0023	27.8
AirTest Technologies	EE80-2CT3		-0.0023	27.8
Automation Components Inc.	ACI/CO2-VDC-R		-0.0022	22.2
Digital Control Systems Inc.	M307		-0.0024	33.3
Greystone Energy Systems Inc.	CDD1A2000		-0.0023	27.8
Honeywell	C7232A1016		-0.0024	33.3
Intec Controls Inc.	I-310E		-0.0026	44.4
Johnson Controls	CD-WA0-00-0		-0.0024	33.3
Senseta	4GS-1		-0.002	11.1
Siemens	QPA2000		-0.0022	22.2
Telaire	Venostat 8001		-0.0023	27.8
Telaire	Venostat 8002		-0.0022	22.2
Vaisala	GMW21		-0.0022	22.2
Veris Industries	CWE SC		-0.0024	33.3
Vulcain	90DM4SM-C-2000		-0.0022	22.2

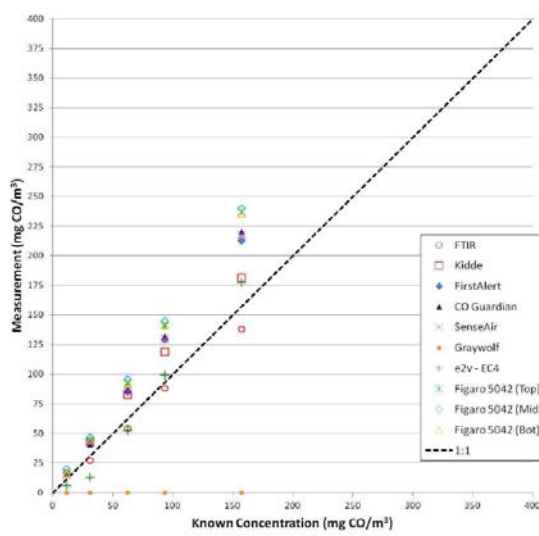
4.2.1.2 *Commercially Packaged Electrochemical CO sensors:* Figure 19 compares the steady state outputs (mg of CO per m<sup>3</sup>) of each commercial sensor against the known concentration of CO in the test chamber for binary test gases of nitrogen and CO in the test chamber pressures indicated. In the ideal case the sensors would output exactly the same CO concentration as the known concentration resulting in linear behavior as shown by the 1:1 line in Figure 19. Most sensors predicted greater amounts of CO in the test chamber at each pressure level than were actually there. Perhaps the factory calibrations were intentionally set conservatively high due to the hazards associated with CO poisoning. Examination of the results shows that each sensor demonstrated a linear response to an increase in the CO concentration. This suggests that the sensors could be recalibrated to provide a more accurate measurement of the steady state CO concentration in the test chamber.



(a)



(b)



(c)

Figure 19. Experimental measurements of CO concentration in nitrogen (mg CO per m<sup>3</sup>) for the electrochemical sensors indicated versus known concentrations in pure nitrogen test gases at the following pressures: (a) 101.3 kPa, (b) 87.5 kPa and (c) 75.3 kPa [33]

The data for the Figaro 5042 sensor are replotted in Figure 20 for nitrogen with CO at test pressures of 101.3, 87.5 and 75.3 kPa. Figure 20 clearly shows a linear response for the Figaro 5042 sensor at each of the pressures. The increasing slope of the sensor response as the pressure is reduced suggests that the accuracy of the sensors decreases slightly as the pressure decreases. However, the sensor behavior is remained linear and appeared predictable.

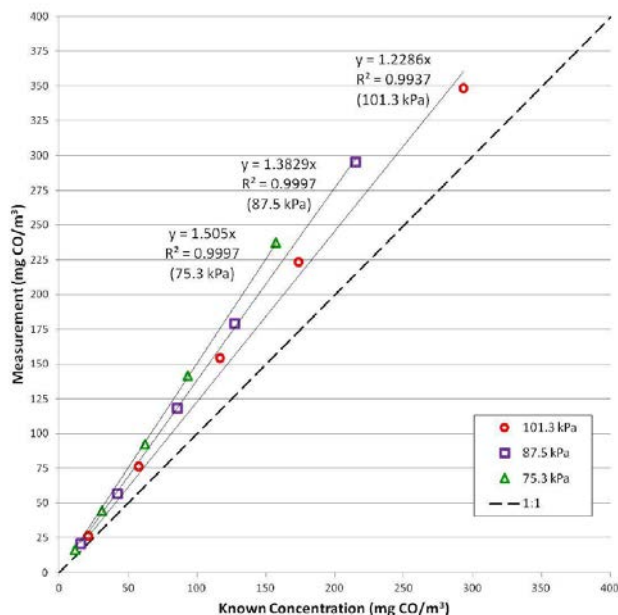


Figure 20. Figaro 5042 sensor response to nitrogen gas with the indicated known concentrations of CO at test pressures of 101.3, 87.5 and 75.3 kPa. [33]

Figure 21 presents the results of repeated experiments on the Figaro 5042 sensor for a steady-state concentration of 233 mg of CO per m<sup>3</sup> in nitrogen-20% oxygen at a pressure of 101.3 kPa. The Figaro 5042 sensors exhibited stable, repeatable steady-state output without any overshoot or undershoot. The responses were quite repeatable in these experiments. The e2v sensor demonstrated a first order response to an increase in the CO concentration with stable, repeatable steady-state output. Unfortunately, the Graywolf sensor malfunctioned and never responded to any of the CO inside the sensor evaluation system.

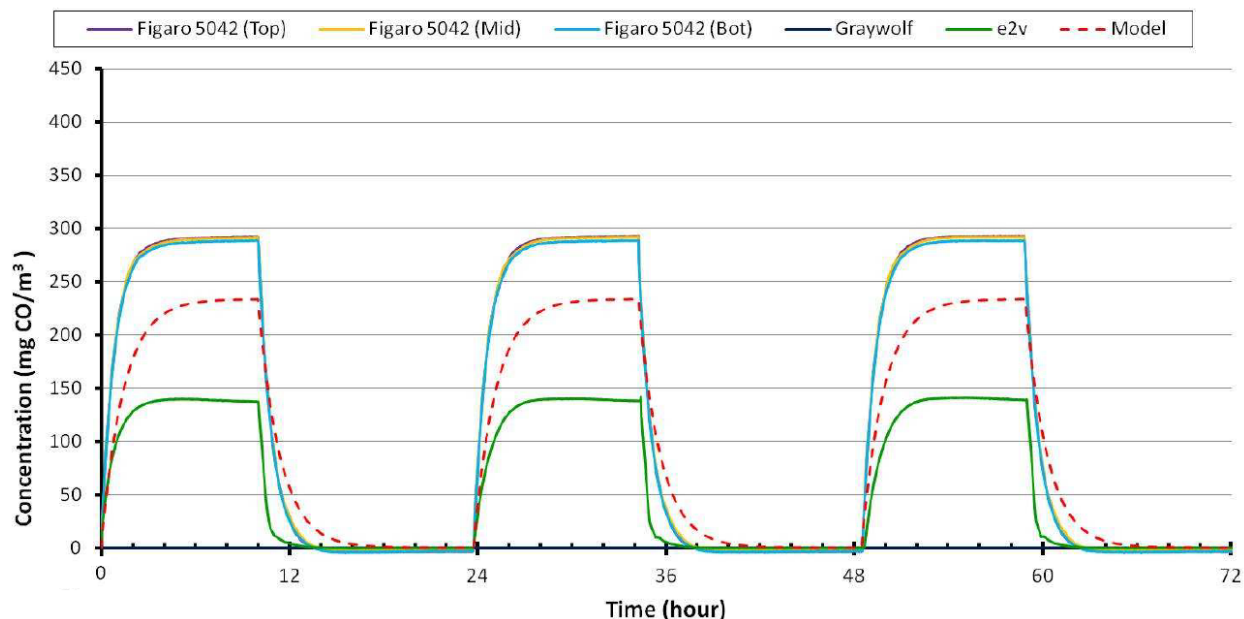


Figure 21. Three repeated transient measurements of CO concentration (known value =  $233 \text{ mg CO/m}^3$ ) in simulated air (80% nitrogen and 20% oxygen) at 101.3 kPa for the electrochemical sensors indicated. The calculated transient test chamber concentration is shown by the dashed line. [33]

## 4.2.2 Transient Responses of Discrete CO<sub>2</sub> Sensors to Calibration Gases

4.2.2.1 *NDIR CO<sub>2</sub> sensors*: Three discrete CO<sub>2</sub> sensors were selected for detailed evaluations of their accuracy and repeatability: Madur madIR-D01 CO<sub>2</sub>, (ii) Figaro K30 sensor and (iii) E2V IR11EJ.[36] The discrete sensors with their evaluation electronics (not commercially packaged instruments as reported in 4.2.1.1) were used so that full access to their control functions and output data could be realized. The discrete sensors were allowed to reach their final steady-state values over a wide range of CO<sub>2</sub> concentrations and then the final ten seconds of each test were averaged to minimize the effect of signal noise and determine the final steady-state concentration. This was the value that was compared to the known concentration of the gas as specified on the gas manufacturer's certificate of analysis.

All three sensors responded linearly and accurately through the range of concentrations tested. The most accurate sensor was the Madur madIR-D01 CO<sub>2</sub> which consistently overestimated the concentration of CO<sub>2</sub> by 1.82 percent. This accuracy was closely followed by the Figaro K30 sensor which underestimated the CO<sub>2</sub> concentration by an average of 1.97 percent. The E2V IR11EJ was the least accurate: typically underestimating the concentration by 4.17 percent.

Table VI provides a summary of the accuracy of each sensor while Table VII provides a summary of the noise detected in the output signal of each sensor. The noise levels ranged from 0.99 PPMV with the Madur madIR-D01 CO<sub>2</sub> to 3.99 ppmv with the E2V IR11EJ. The results

correspond to the range of the analogue voltage outputs. With a larger output range, the same variation in voltage levels corresponds to a smaller change in concentration. Therefore, the signal from the Madur madIR-D01 CO<sub>2</sub> with an analogue voltage output which ranges from 0 to 10 VDC had the least noise while the signal from the E2V IR11EJ with a voltage output ranging from 0 to 2.048 VDC was the noisiest.

**Table VI**  
**Summary of the Accuracy of Each Discrete CO<sub>2</sub> Sensor**  
 (0 to 1889 ppmv)

Sensor	Tests	Span Error (%)	0 PPMV Offset Error (ppmv)
Madur madIR-D01 CO <sub>2</sub>	24	+ 1.82	+ 13.1
Figaro K30	21	- 1.97	- 1.4
E2V Ir11EJ	36	- 4.17	-12.7

**Table VII**  
**Summary of RMS Noise evaluation of Each Discrete CO<sub>2</sub> Sensor**

Sensor	Number of Tests	RMS Noise (mV)	STDEV (mV)	RMS Noise (PPMV)	STDEV (PPMV)
MADUR madIR-D01 CO <sub>2</sub>	18	3.96	4.68	0.99	1.17
E2V IR11EJ	15	4.33	1.11	3.99	1.02
Figaro K30	26	6.46	3.62	3.23	1.81

The amount of noise can be reduced considerably with minimal loss of information using a simple running average technique. The data acquisition system has a sampling rate of 60 Hz which easily exceeds the 1 Hz update rate of the sensor. Consequently, it is possible to perform a running average over a one second interval and retain all the features of the data while reducing the noise. Table VIII shows the effect of the running average at reducing the RMS noise present in the signal output. The greatest effect was to reduce by 87% the noise present in the Figaro sensor, a decrease from 3.23 ppmv to 0.41 ppmv.

**Table VIII**  
**Summary of RMS Noise of Each Discrete CO<sub>2</sub> Sensor**  
 (1 second running average)

Sensor	Number of Tests	RMS Noise (PPMV)	STDEV (PPMV)
MADUR madIR-D01 CO <sub>2</sub>	18	0.65	1.26
E2V IR11EJ	15	3.08	0.92
Figaro K30	26	0.41	0.73

The limit of detection is the smallest change in concentration which can be reliably distinguished from the background noise of the signal as shown schematically in Figure 22. Three times the sensor’s RMS noise was adopted as the limit of detection as is commonly utilized in analytical chemistry. Table IX summarizes the limits of detection for each of the sensors based on the 1 second RMS noise limit. Table X shows the T90 response times (time to reach 90% of the new steady state response) for the sensors.

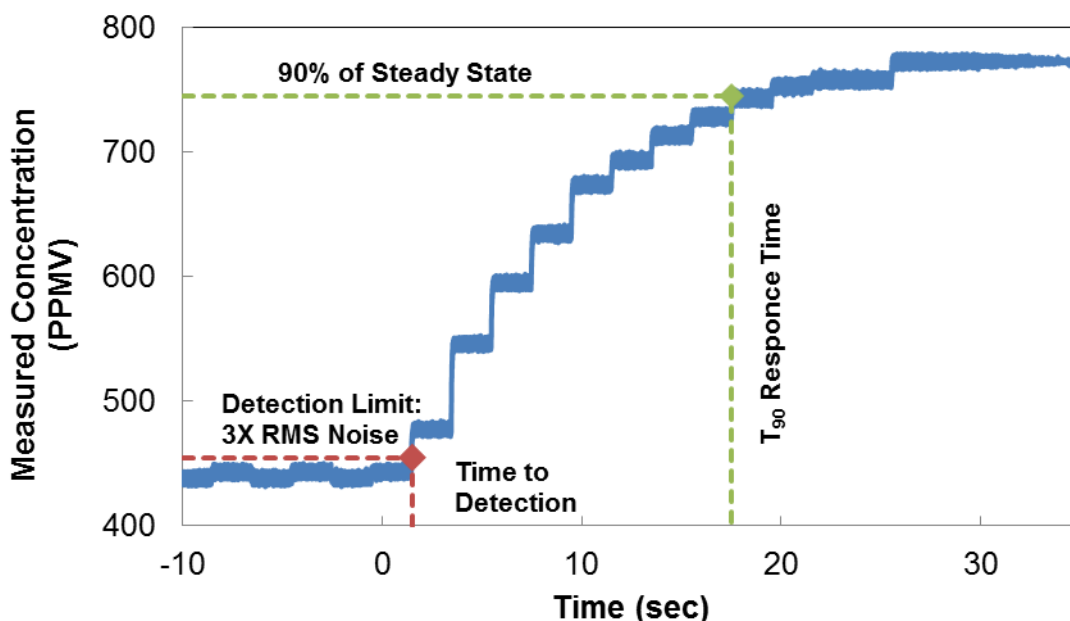


Figure 22. Schematic response of a NDIR CO<sub>2</sub> sensor to a flowing gas experiment illustrating the two transient parameters: (i) time to detection and (ii) time to reach 90% of the new steady state concentration (T<sub>90</sub>). The gas concentration is instantaneously changed to a new steady value when the time = zero.

**Table IX**

**Limits of Detection for Each Discrete CO<sub>2</sub> Sensor**

Sensor	RMS Noise (PPMV)	Limit of Detection (PPMV)
MADUR madIR-D01 CO <sub>2</sub>	0.99	2.97
E2V IR11EJ	3.99	11.97
Figaro K30	3.23	9.69

**Table X**

**T<sub>90</sub> Response Times for Each Discrete CO<sub>2</sub> Sensor**

Sensor	Number of Tests	Rise Time 0-90% (sec)	STDEV (sec)
Madur madIR-D01 CO <sub>2</sub>	18	24.90	0.25
E2V IR11EJ (micropump)	20	13.46	1.79
Figaro K30 (micropump)	6	18.76	0.36

4.2.2.2 *Electrochemical CO sensors:* Three discrete CO sensors were selected for detailed evaluations of their accuracy and repeatability: (i) M TGS5042, (ii) E2V EC4-500-CO and (iii) Alphasense CO-B4.[35] As with the discrete CO<sub>2</sub> sensors, discrete CO sensors with their evaluation electronics (not commercially packaged instruments reported in 4.2.1.2) were used for full control of sensor performance and access to their output data. The discrete sensors were allowed to reach their final steady-state values over a wide range of CO concentrations and then the final ten seconds of each test were averaged to minimize the effect of signal noise and determine the final steady-state concentration. This was the value that was compared to the known concentration of the gas as specified on its manufacturer’s certificate of analysis.

The steady state responses of all three CO sensors are shown in Figure 23. The solid line indicates a 1:1 ratio where the sensor reading would be identical to the actual gas concentration.

All three sensors lie very close to the 1:1 relationship. The Alphasense CO-B4 sensor was only tested for the three lowest concentrations of test gas and exhibited the highest sensitivity of the three sensors investigated.

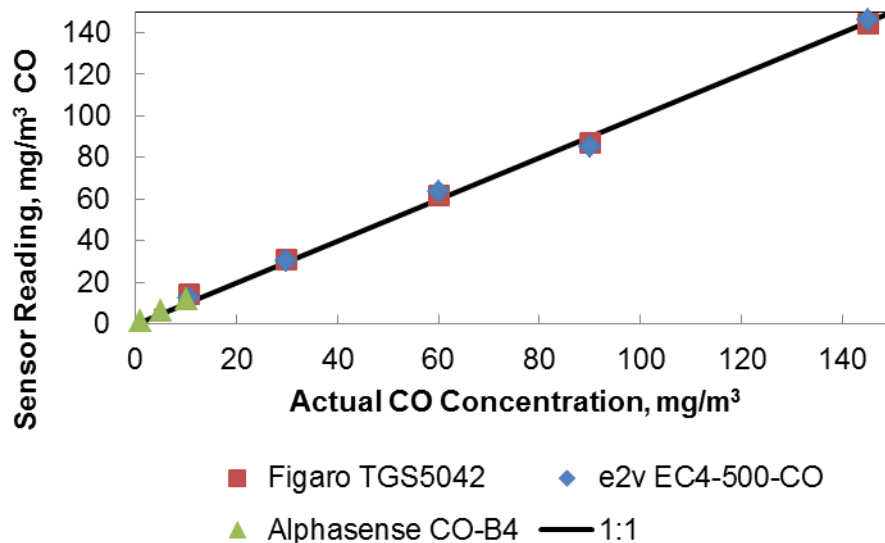


Figure 23. Steady state comparison of the CO-B4 (triangles), Figaro TGS5042 (squares), and e2v EC4-500-CO (circles). The sensor readings were compared with the actual concentration and the ideal 1:1 relationship (solid).

The T90 response times and minimum detection times for the three discrete CO sensors are shown in Table XI. e2v EC4-500-CO sensor are shown in Table XI. The mean rise time for the Figaro TGS5042 and the E2V EC4-500-CO sensors are similar (11.5 and 14.3 s, respectively). However, the Alphasense CO-B4 takes 2-3 times longer to reach steady state presumably due to the signal averaging technology utilized in this very sensitive device. Interestingly, the event detection times of the three sensors are all similar.

**Table XI**

**Transient Performance for Discrete CO Sensors**

Sensor	T90 Rise Time (s)	Detection Time (s)
Figaro TGS5042	11.5	2.4
E2V EC4-500-CO	14.3	1.4
Alphasense CO-B4	33.8	2.2

### 4.3 Commercial Sensors Responses to Fumes from Mobil Jet Oil II

One gram of Mobil Jet Oil II was thermally degraded in the bell jar shown previously in Figure 6(d). The furnace target maximum temperature was set to 375°C and a heating rate of 10°C/min was utilized to heat the oil sample. The oil began to lose mass after approximately 30 minutes and at a temperature of approximately 190°C. White smoke was observed at that time and the amount of smoke increased as the experiment progressed as shown in Figure 24. The oil reached and maintained a steady state temperature of 225°C during the time that mass loss and smoke generation continued. At the end of the experiment, only charred black material remained in the crucible.

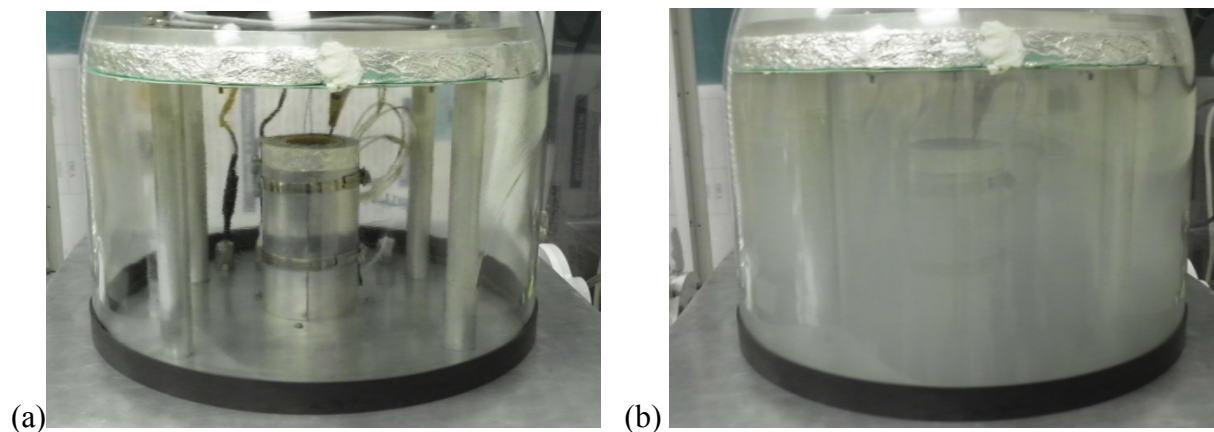


Figure 24. a) Bell jar before thermally degrading 1g of Mobil Jet Oil II; b) smoke-filled bell jar during degradation experiment.

Figures 25 and 26 show the change of CO and CO<sub>2</sub> concentration as a function of time along with the Mobil Jet Oil II mass change. The sensors began detecting CO and CO<sub>2</sub> at approximately the same time that significant mass loss began (~30 minutes). The downstream FTIR began detecting changes in the air samples about 5 minutes later. The measured concentrations from the sensors and the FTIR appear to reach maximum values near the end of the thermal degradation. Interestingly, although the downstream FTIR detection of CO shown in Figure 25 began to decrease after the upstream electrochemical sensor, as expected, the FTIR detection of CO<sub>2</sub> began to decrease before the upstream NDIR CO<sub>2</sub> sensor as shown in Figure 26. This behavior may be due to smoke particles coating the NDIR sensor optics during the experiment.

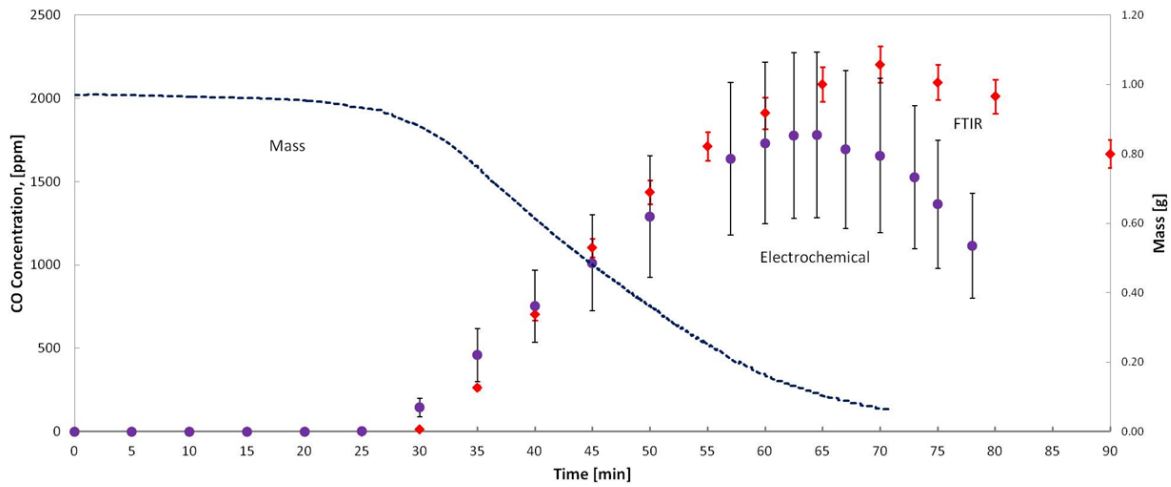


Figure 25. Plot of the change in CO concentration as a function of time as measured by the TGS5042 sensor (circles) and the FTIR (diamonds) and the mass (dashes) as a function of time.

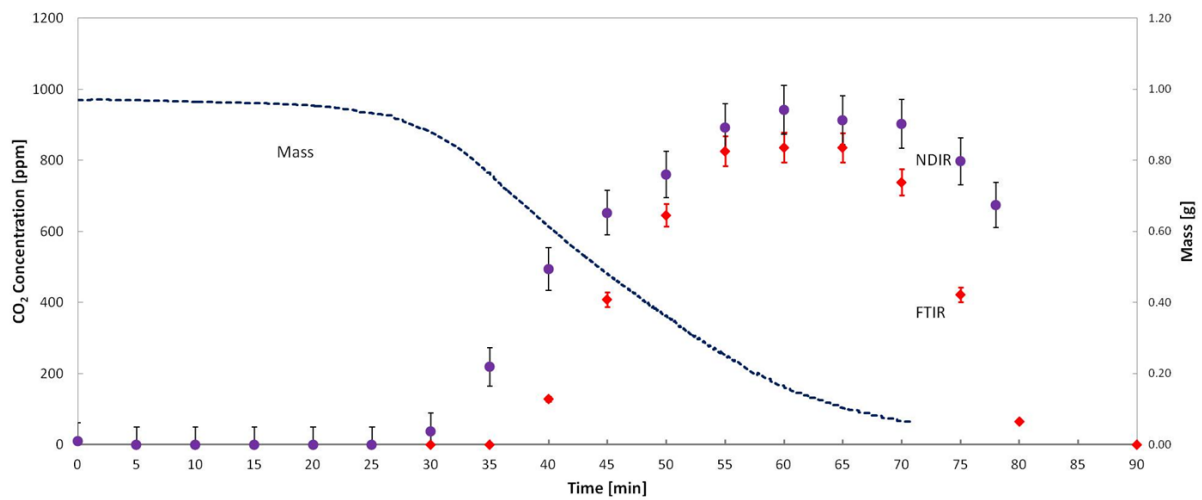


Figure 26. Plot of the CO<sub>2</sub> concentration as a function of time as measured by the EE80 (circles) and the FTIR (diamonds) and the mass (dashes) as a function of time.

#### **4.4 Detection of Bleed Air Contamination from Mobil Jet Oil II Injection into the AP1 Port of a Pratt & Whitney F117/PW2000 Turbofan Engine**

In 2011 Auburn University began collaborating with scientists and engineers from NASA Glenn Research Center, NASA Dryden Flight Research Center, FAA Tech Center, Boeing, Pratt & Whitney and Kansas State University (among other organizations) to plan and develop a test system for injecting engine oil into the compressor of a modern turbofan engine and then evaluating any resultant contamination of the engine's bleed air supply. The bleed air testing was integrated within a larger NASA test program called the Vehicle Integrated Propulsion Research (VIPR) Project that was developing engine health diagnostic techniques and evaluating the effects of volcanic ash simulants ingested by the test engine. All testing was accomplished on the ground at Edwards Air Force Base in California using an Air Force C17 powered by four Pratt & Whitney F117/PW2000 engines.

Auburn University's role in the bleed air contamination activity was twofold: (1) develop the oil injection system to reliably inject precise quantities of oil into the compressor of the F117/PW2000 engine and (2) evaluate the ability of low cost, commercial sensor technology to detect the contamination event. Figure 27(a) shows a drawing of the aircraft test configuration. One of the engines of the C17 was removed and modified for the VIPR Project. After the engine modifications were completed, the engine was reinstalled on the aircraft. The modifications enabled the bleed air supply from the engine to be routed to a series of test stations located under the engine and protected by a large circular platform as shown. All testing was computer controlled by scientists and engineers located in the C17 over a two day period in July 2015.

A schematic of the Auburn University oil injection system and the bleed air sensor system is shown in Figure 27(b). Figure 28 presents photographs of the actual oil injection system hardware and the commercial sensor test system, both located underneath the protective circular platform.

The commercial NDIR carbon dioxide sensors and electrochemical carbon monoxide sensors selected for the testing are listed in Table XII. These are the same technologies evaluated in the transient tests reported above in Section 4.2.2. In addition, two commercial methane sensors (catalytic bead pellistor technology [37]) and a commercial smoke detector (with both an ionization sensor and a photoelectric sensor) were also utilized in the bleed air sensor package.

Test Day 1 on July 8, 2015 saw attempts to inject Mobil Jet Oil II into the engine's AP1 borescope view port using injection rates of 3.33, 6.67, 10.0 and 13.3 grams per minute for 10 minute durations. The oil injector nozzle temperature varied from 200-220°F during the tests. Unfortunately the very small 0.0058 inch diameter orifice of the oil injector apparently experienced clogging issues during the first day and testing had to be suspended to replace it.

A back-up injector with an orifice diameter of 0.0087 inch diameter was installed for the testing activity during the second day and no further clogging issues occurred. Three tests involving an oil injection rate of 20 grams per minute for 28 minute durations were selected for Test Day 2 (July 9, 2015).

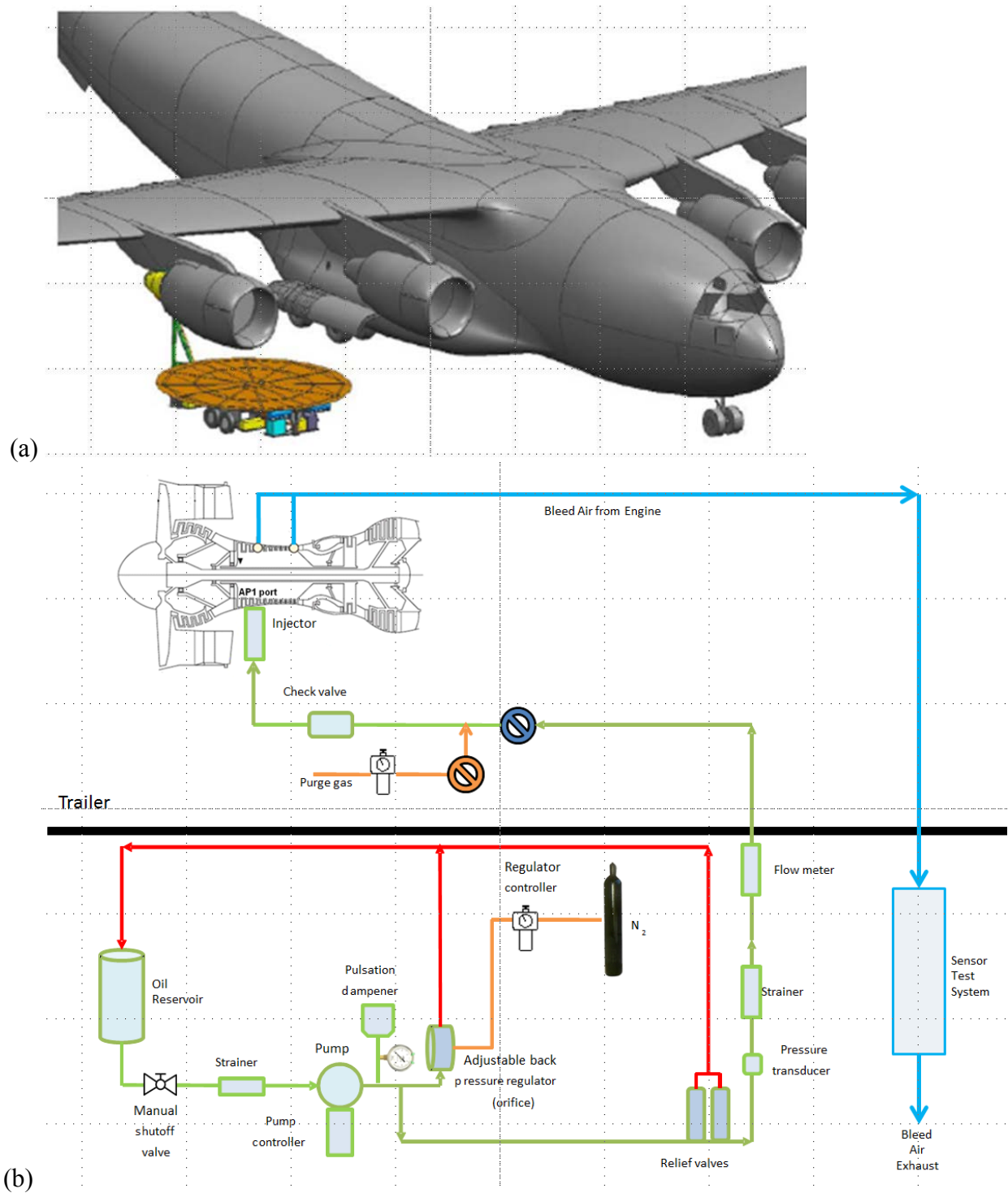


Figure 27. (a) Overall configuration of the C17 engine test systems. (b) Schematic of the layout for the oil injection system and the commercial sensor bleed air test system.

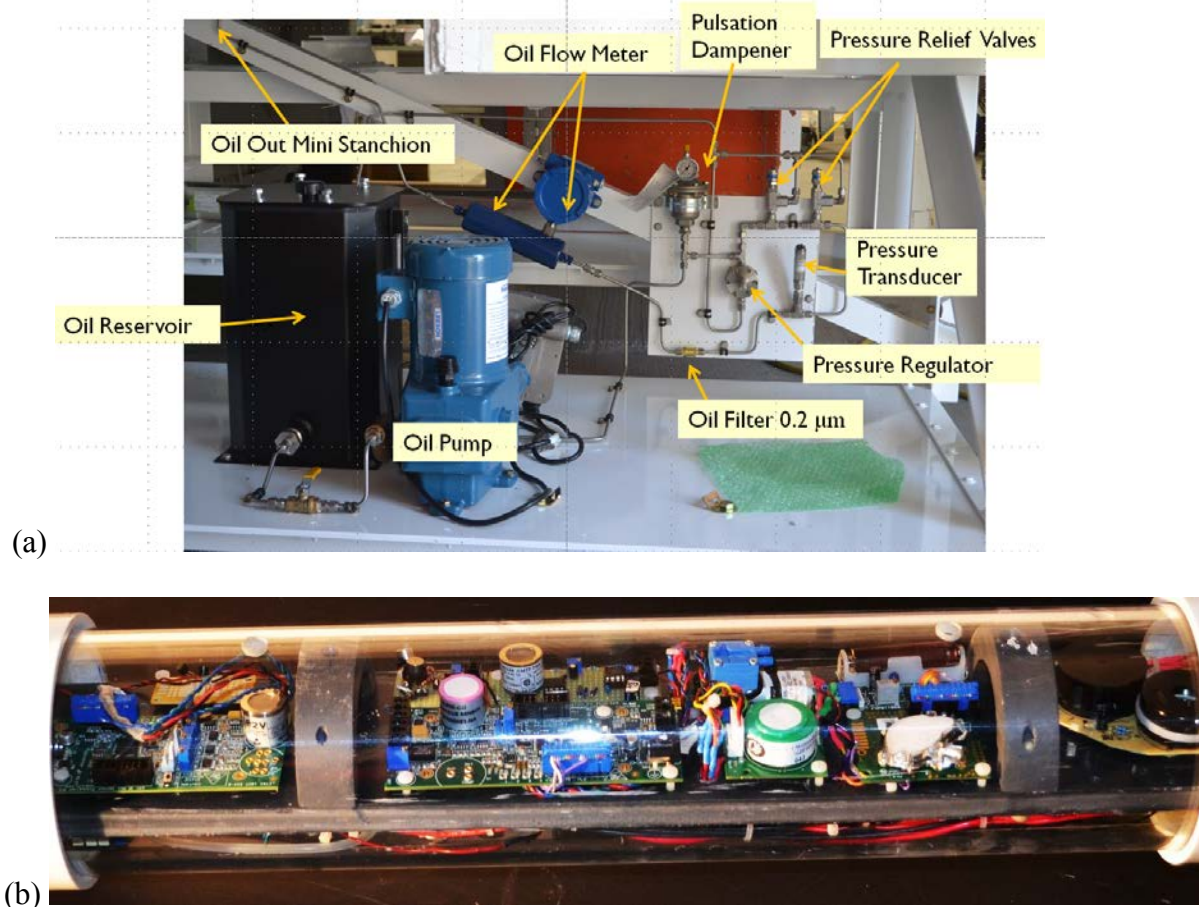


Figure 28. (a) Picture of the main components of the oil injection system.  
 (b) Picture of the commercial sensor test system.

**Table XII**  
**Commercial Sensors Evaluated in the VIPR Bleed Air Contamination Tests**

Electrochemical Carbon Monoxide Sensors: 1) Figaro 5042 2) e2v EC4-500 3) Alphasense CO-B4	NDIR Carbon Dioxide Sensors: 1) Madur madIR-D01 2) e2v IR11EJ 3) Figaro K30
Pellistor Methane Sensor: 1) Alphasense CH-A3 2) e2v VQ10SB	Smoke Detector: 1) Kidde # PI9010

The only commercial sensor from the entire group that reliably reacted to changes in the bleed air quality due to the oil injections was the Alphasense CO-B4. The CO-B4 is a high sensitivity, electrochemical device that is marketed for use where ppb detection levels of CO are required. With the manufacturer's stated lower detection limit of less than 20 ppb, the sensor incorporates technology to maximize signal-to-noise ratio and low zero currents. Figure 29 shows the amounts of carbon monoxide detected by the Alphasense CO-B4 sensor (upper curve) as well as the measured amounts of oil injected into the engine (lower curve) during the tests that occurred on Day 1. As noted above, partial clogging of the miniature oil injector nozzle caused poor control of the amount of oil injection. Steady 10 min oil injections (3.33, 6.67, 10.0 and 13.3 g/min) were attempted but not realized for any test. The maximum oil injection achieved was measured as approximately 12 g/min. Nevertheless, the sensor did appear to react to the oil injection and began to respond at an oil injection rate of ~10 g/min.

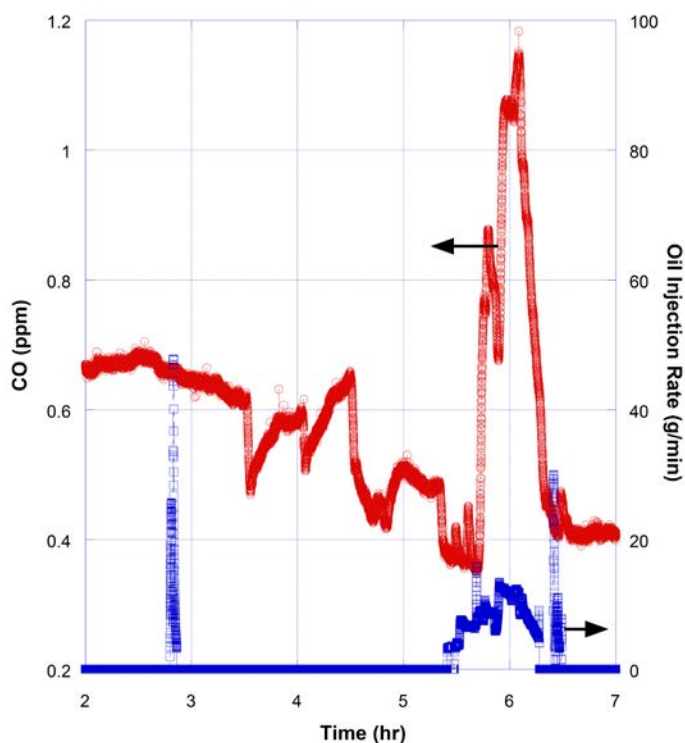


Figure 29. Amounts of carbon monoxide (CO) detected with the Alphasense CO-B4 high sensitivity sensor (upper curve) and the measured amounts of oil injected into the engine (lower curve) during Day 1 of the VIPR tests. Partial clogging of the miniature oil injector nozzle caused poor control of the amount of oil injection.

Figure 30 shows the amounts of carbon monoxide detected by the Alphasense CO-B4 sensor (upper curve) as well as the measured amounts of oil injected into the engine (lower curve) during the three tests that occurred on Test Day 2. A constant oil injection rate of 20 grams per minute for 28 minute durations were utilized during Test Day 2. The engine was then run for approximately 30 minutes without any oil injection between the oil injection tests to ensure that all oil from the previous test was burned out of the engine prior to the next test. The CO-B4

sensor was well behaved during the three 20 g/min tests of Day 2 and reliably detected the presence of ~1 ppm CO in the bleed air stream during each oil injection experiment. The average delay between the initiation of the oil injection into the AP1 port on the engine and the beginning of the sensor response was approximately 4.5 minutes. This sensor appears to have merit for potential application as a low cost bleed air contamination detector and further test and evaluation is recommended.

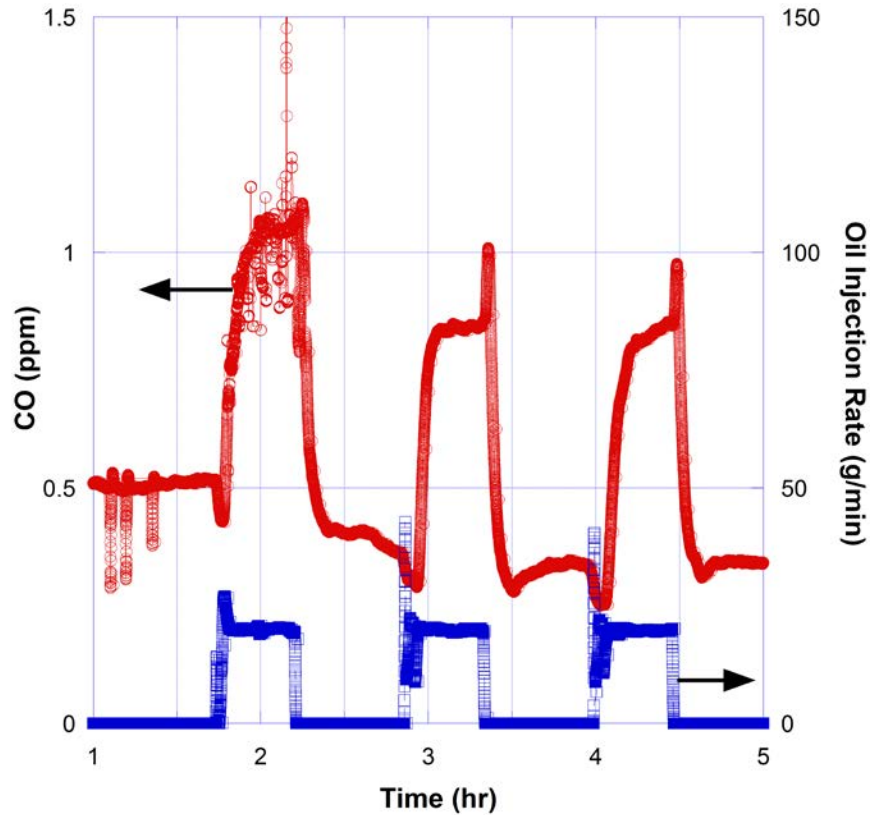


Figure 30. Amounts of carbon monoxide (CO) measured using the Alphasense CO-B4 high sensitivity sensor (upper curve) and the measured amounts of oil injected into the engine (lower curve) during Day 2 of the VIPR tests.

## 5.0 Conclusions

14 CFR 25.831 states that aircraft air must be free from harmful or hazardous concentrations of gases or vapors and places specific limits on the following: carbon monoxide (<50 ppmv) and carbon dioxide (<5000 ppmv). Even with these specific allowable limits, there are currently no requirements for real-time monitoring of either of these contaminants on aircraft.

The current investigation has evaluated the applicability of low cost, commercial sensor technologies for detecting carbon dioxide (CO<sub>2</sub>) using non-dispersive infrared technologies and carbon monoxide (CO) using electrochemical sensing technologies in aircraft cabins and bleed air systems. Both methods offer considerable promise for aircraft cabin measurements of these gaseous contaminants in the range of limits imposed by the FAA through 14 CFR 25.831. However, existing sensor packaging and maintenance/calibration methods must be adapted to the unique environment and more stringent performance requirements anticipated for aircraft. In addition, the high sensitivity and response time of the Alphasense CO-B4 carbon monoxide sensor enabled detection of carbon monoxide in the bleed air supply from controlled injections of Mobil Jet Oil II (10 g/min – 20 g/min) into the AP1 borescope port of a Pratt & Whitney F117/PW2000 engine. This sensor technology appears to have considerable potential for further development into a detector for oil contamination of aircraft bleed air supplies.

## 6.0 Acknowledgments

This project was funded by the U.S. Federal Aviation Administration (FAA) Office of Aerospace Medicine through the National Air Transportation Center of Excellence for Research in the Intermodal Transport Environment (RITE), Cooperative Agreements 07-C-RITE and 10-C-RITE. Although the FAA has sponsored this project, it neither endorses nor rejects the findings of this research.

## 7.0 References

- [1] NRC (National Research Council); 2002, The Airliner Cabin Environment and the Health of Passengers and Crew, Washington, DC, National Academy Press.
- [2] “De-icing solution sends air crew members to hospital,” *CNN*, 24 Dec 2008.
- [3] Crane, Charles R., Sanders, Donald C., Endecott, Boyd R., Abott, John K., “Inhalation Toxicology: III Evaluation of Thermal Degradation Products from Aircraft and Automobile Engine Oils, Aircraft Hydraulic Fluid, and Mineral Oil,” FAA-AM-83-12, 1983.
- [4] Van Netten, Chris, “Aircraft Air Quality Incidents, Symptoms, Exposures and Possible Solutions,” in Air Quality in Airplane Cabins and Similar Enclosed Spaces, *Hdb Env. Chem.* Vol. 4, Part H (Springer, Berlin) 2005, pp. 192-210.
- [5] Shayne, B., “Plane with sick passengers had air contamination before,” *WCNC*, 20 Jan 2010.
- [6] Abou-Donia, M.B., “Organophosphorous ester-induced chronic neurotoxicity,” *Arch. Environ. Health*, 2003, Vol. 58, pp. 484-497.
- [7] Winder, Chris and Balouet, Jean-Christophe, “The Toxicity of Commercial Jet Oils,” *Environ. Res. A*, 2002, 89, pp. 146-164.
- [8] Watson, Jean; 2009, personal communication.
- [9] J.T.L. Murawski, J.T.I. and Supplee, D.S., “An Attempt to Characterize the Frequency, Health Impact and Operational Costs of Oil in the Cabin and Flight Deck on U.S. Commercial Aircraft,” *J. ASTM Intl* , 2008, Vol. 5, No. 5, Paper ID JAI101640.
- [10] Department of Transportation, Bureau of Transportation Statistics, [http://www.bts.gov/publications/national\\_transportation\\_statistics/html/table\\_01\\_37.html](http://www.bts.gov/publications/national_transportation_statistics/html/table_01_37.html), accessed February 3, 2012
- [11] “Air Quality within Commercial Aircraft,” ANSI/ASHRAE Standard 161-2007, American Society of Heating, Refrigerating, and Air-Conditioning Engineers, 2008, Atlanta, GA.
- [12] Hunt, Elwood H., Reid, Don H., Space, David R. and Tilton, Fred E., “Commercial Airliner Environmental Control System,” Aerospace Medical Association Annual Meeting, 1995, Anaheim, CA, USA.
- [13] Jones, Byron, personal communication, 2011.
- [14] van Netten, C., Leung, V., “Hydraulic Fluids and Jet Engine Oil: Pyrolysis and Aircraft Air Quality,” *Archives of Environmental Health*, 2001, 56(2): p. 181-186.
- [15] van Netten, C., Multi-elemental Analysis of Jet Engine Lubricating Oils and Hydraulic Fluids and Their Implication in Aircraft Air Quality Incidents., *The Sci. of the Total Environ.*, 1999, 229, p. 125-129.

- [16] van Netten, C., Leung, V., “Comparison of the Constituents of Two Jet Lubricating Oils and Their Volatile Pyrolytic Degradation Products,” Applied Occupational and Environmental Hygiene, 2000, 15(3): p. 277-283.
- [17] Crane, C.R., Sanders, D.C., Endecott, B.R., Abbott, J.K., “Inhalation Toxicology: III. Evaluation of Thermal Degradation Products from Aircraft and Automobile Engine Oils, Aircraft Hydraulic Fluid and Mineral Oil,” FAA Civil Aeromedical Institute, FAA-AM-83-12, 1983.
- [18] Bartl, P., Volkl, C., Kaiser, M., “Chemical Characterization of Polyol Ester Aviation Lubricant Residues,” J. Synthetic Lubrication, 2008, 25, p. 1-16.
- [19] Jones, E., “The pellistor catalytic bead sensor,” in Solid State Gas Sensors, Moseley, P.T. and Tofield, B.C., Eds., 1987, Institute of Physics, Bristol, UK, p. 17-31.
- [20] Korotcenkov, G., “One-electrode Semiconductor Gas Sensors,” in Science and Technology of Chemiresistor Gas Sensors, Aswal, D.K. and Gupta, S.K., Eds, 2007, Nova Science Publishers, New York, USA, p. 95-145.
- [21] Chou, J., Hazardous Gas Monitors, 1999, McGraw Hill, New York, USA, p. 37-41.
- [22] Kaur, M., Aswal, D.K., Yakhmi, J.V., “Chemiresistor Gas Sensors: Materials, Mechanisms and Fabrication,” in Science and Technology of Chemiresistor Gas Sensors, Aswal, D.K. and Gupta, S.K., Eds, 2007, Nova Science Publishers, New York, USA, p. 33-93.
- [23] Stetter, J.R., Li, J., “Amperometric Gas Sensors – A Review,” Chem. Rev., 2008, 108, p. 352-366.
- [24] Fergus, J.W., “Solid electrolyte based sensors for the measurement of CO and hydrocarbon gases,” Sensors and Actuators B, 2007, 122, p. 683-693.
- [25] Fergus, J.W., “A review of electrolyte and electrode materials for high temperature electrochemical CO<sub>2</sub> and SO<sub>2</sub> gas sensors,” Sensors and Actuators B, 2008, 134, p. 1034-1041.
- [26] Verner, P., “Photoionization detection and its application in gas chromatography,” J. Chromatography, 1984, 300, p. 249-264.
- [27] Shrestha, S.S. and Maxwell, G.M., 2009, “Product Testing Report – Wall Mounted Carbon Dioxide Transmitters,” National Building Controls Information Program, Iowa Energy Center (Ankeny, IA).
- [28] Shrestha, S.S. and Maxwell, G.M., 2009, “An experimental evaluation of HVAC-grade carbon dioxide sensors: Part 1, test and evaluation procedure,” ASHRAE Transactions, 115(2).
- [29] Shrestha, S.S. and Maxwell, G.M., 2010, “An experimental evaluation of HVAC-grade carbon dioxide sensors: Part 2, performance test results,” ASHRAE Transactions, 116(1).
- [30] Shrestha, S.S. and Maxwell, G.M., 2010, “An experimental evaluation of HVAC-grade carbon dioxide sensors: Part 3, humidity, temperature and pressure sensitivity test results,” ASHRAE Transactions, 116(1).
- [31] Beta, I.A., “TGA Measurements of Oil Samples with Evolved Gas Analysis by FTIR and MS,” 2011, Report No. 621002184, NETZSCH Instruments North America, LLC (Burlington, MA).
- [32] Haney, R.L., “Principal Component Analysis for Enhancement of Infrared Spectra Monitoring,” 2011, Ph.D. Dissertation, Auburn University, Auburn, AL.

- [33] Andress, J.R., "Evaluation and Analysis of Commercially Available Electrochemical Carbon Monoxide Sensors for Aircraft Applications," 2012, M.S. Thesis, Auburn University, Auburn, AL.
- [34] Neer, R.L., "Development of a Laboratory Apparatus to Study the Thermal Degradation Behavior of Jet Engine Oils," 2012, M.S. Thesis, Auburn University, Auburn, AL.
- [35] Buck, A.L., "Steady State and Transient Response Characteristics of Commercial Carbon Monoxide Sensors," 2014, M.S. Thesis, Auburn University, Auburn, AL.
- [36] Roberts, M.I., "Steady State and Transient Response Characteristics of Commercial Non-Dispersive Infrared Carbon Dioxide Sensors," 2014, M.S. Thesis, Auburn University, Auburn, AL.
- [37] Brooks, B.C., "Transport Modeling and Response Characteristics of Commercial Catalytic Bead Sensors," 2015, M.S. Thesis, Auburn University, Auburn, AL.